ACADEMIA DA FORÇA AÉREA

Effect of Radiation-Assisted Cure on the Functional Properties of Carbon-Epoxy Composites

Luís Filipe da Costa Paulino

ASPAL/PILAV/140677-K

Dissertation to obtain the Master of Science Degree in

Military and Aeronautical Sciences – Aviator Pilot

Examination Committee

President: COR/PILAV Luís Miguel Gomes Graça

Supervisor: MAJ/ENGAED Luís Filipe Magalhães Pereira

Co-supervisor: Professor Doutor Luís Miguel Mota Ferreira

Member: Professor Doutor João Paulo Leal

Sintra, May 2022

INTENTIONALLY LEFT BLANK

Acknowledgments

I would like to thank my supervisors, Major Luís Pereira and Professor Luís Ferreira, for the extraordinary support and motivation provided to me when I was feeling lost during this dissertation and for the time they spent teaching me completely new subjects. Furthermore, they were always available to answer my questions and help me solve every problem that came up. Without them, I would not have been able to complete this dissertation.

The laminate fabrication would have been impossible without the help of Sargento-Chefe Paulo Mendes and Alferes Vasco Coelho. Sargento-Chefe Mendes transmitted all the necessary knowledge to fabricate the laminates and was always available to offer a helping hand to solve any setback. Furthermore, Alferes Coelho willingly gave up his own time to help fabricate the laminates when I was not able to, which was essential to continue this dissertation.

I would also like to thank Dr. Pedro Santos from the C^2TN Experimental Irradiation Facility (IRIS), who operated the Cobalt-60 irradiator and conducted the innumerous irradiations necessary for this dissertation and Dra. Helena Casimiro for teaching me how to operate the DSC in order to determine the glass transition temperature.

To my family for motivating me and helping me with everything they could, and to my friends for supporting me and understanding my absence during this period.

Finally, to KAISERS, who accompanied me in the last 5 years in the academy, for their support, for all the experiences we had together, and for helping me grow and become the person I am today.

Obrigado a todos!

INTENTIONALLY LEFT BLANK

Abstract

Gamma radiation has been successfully used to improve polymer's properties. In this regard, this study aims to assess if it is possible to improve carbon-epoxy composites' mechanical and thermal properties, with potential application in aeronautics, through controlled exposition to gamma radiation. In addition, make a comparative study between post-cure irradiation and radiation-assisted cure. To accomplish this, the material is subjected to gamma radiation in different stages of the resin's cure.

The laminates were fabricated with a 3K carbon mat with 160 $g.m^{-2}$ and a two-component resin SR8200 with SD7206 hardener through wet-layup. The test specimens were cut from the laminate according to ISO 527-4/2020 and ISO 14125/2011. Finally, they were irradiated according to three irradiation methodologies: post-cure irradiation, irradiation after 2 days, and after 10 days with doses from 4 to 7 kGy. These doses were selected based on a preliminary study.

The specimens were tested through tensile and flexural testing, thermogravimetry analysis and differential scanning calorimetry. The results showed that up to 6 kGy, the three irradiation methodologies improved the thermal stability and mechanical properties without affecting molecular structural integrity due to chain-scission, compared to non-irradiated specimens.

The biggest increases registered were a 32.36 % increase in Young's modulus and a 51.23 % increase in flexural modulus for irradiation after 2 days, and an increase of 5.10 % in degradation temperature and 7.44 % in glass transition temperature for the same irradiation methodology, suggesting that radiation-assisted cure is more effective at improving the material's properties compared to post-cure irradiation.

Keywords: Radiation-assisted cure, carbon-epoxy, composites, crosslinking, mechanical properties, thermal properties

INTENTIONALLY LEFT BLANK

Resumo

A radiação gama tem sido utilizada na melhoria das propriedades de polímeros. Desta forma, este estudo visa avaliar a possibilidade de melhorar as propriedades mecânicas e térmicas dos compósitos carbono-epóxi, para aplicação na aeronáutica, por exposição controlada à radiação gama. Adicionalmente, realizar um estudo comparativo entre a irradiação pós-cura e a cura assistida por radiação. Para tal, o material foi submetido a radiação gama em diferentes fases da cura da resina.

Os laminados foram fabricados com uma tela de carbono 3K com 160 $g.m^{-2}$ e uma resina SR8200 misturada com o endurecedor SD7206 através de *wet-layup*. As amostras foram cortadas conforme as normas ISO 527-4/2020 e ISO 14125/2011 e irradiadas segundo três metodologias: irradiação pós-cura, irradiação após 2 dias, e após 10 dias com doses de 4 a 7 kGy, selecionadas num estudo preliminar.

As amostras foram testadas através de ensaios de tração e flexão, análise termogravimétrica e calorimetria diferencial de varrimento. Os resultados revelaram que até 6 kGy, as três metodologias de irradiação melhoraram a estabilidade térmica e as propriedades mecânicas, sem afetar a integridade estrutural molecular devido à cisão em cadeia, comparativamente às amostras não irradiadas.

Os maiores aumentos foram registados na irradiação após 2 dias, traduzindo-se num aumento de 32.36 % no módulo de Young, 51.23 % no módulo de flexão, 5.10 % na temperatura de degradação e 7.44 % na temperatura de transição vítrea, sugerindo que a cura assistida por radiação é mais eficaz na melhoria das propriedades do material comparativamente à irradiação pós-cura.

Palavras-chave: Cura assistida por radiação, carbono-epóxi, compósitos, reticulação, propriedades mecânicas, propriedades térmicas

INTENTIONALLY LEFT BLANK

Table of Contents

List of Figures

List of tables

List of Abbreviations

ASTM	American Society for Testing Materials
C^2TN	Center for Nuclear Sciences and Technologies
CIAFA	Investigation Center of the Portuguese Air Force Academy
CNC	Computer Numerical Control
D	Absorbed Dose
DGEBA	Diglycidyl Ether of Bisphenol A
DSC	Differential Scanning Calorimetry
DU	Dose Uniformity
E-Beam	Electron Beam
IRIS	Ionizing Radiation Facilities laboratory
ISO	International Organization for Standardization
LME	*Laboratório de Mecânica Experimental*
PMMA	Polymethyl Methacrylate
STD	Standard Deviation
TA	Thermal Analysis
T_{deg}	Degradation Temperature
T_g	Glass Transition Temperature
TGA	Thermogravimetric Analysis
U	Dose Uniformity
UAV	Unmanned Aerial Vehicle
UV	Ultraviolet

INTENTIONALLY LEFT BLANK

1 Introduction

1.1. Background and Motivation

The advent of composite materials that combine stiff fibers, such as carbon fiber, with high-performance polymer resins has been helping to overcome major difficulties posed by the complex design of modern aircraft. The advantage of composites compared to metals is the manufacturing process that allows complex shapes to be fabricated with lower density, resulting in a lighter material offering a lower fuel consumption for aviation and automobile industries (Hsissou et al., 2021).

Fiber-reinforced polymer composite materials are becoming the primary choice material for aircraft construction. Current military and civil airplanes, helicopters, satellites and missile development programs use composites as prime materials, demonstrating their enormous potential (Mangalgiri, 1999). The aviation industry is the most interested and constantly adapting to integrating composites to enhance performance and safety. The aviation industry includes not only commercial and private aircraft but also military and aerospace. A profitable aviation business depends on stronger lightweight materials for their aircraft without compromising safety and reliability (Yadav et al., 2021).

Modern military aircraft have over 30 % of their structural weight built-in advanced composites (wings, propellers, control surfaces and radome). Modern civil aircraft, such as Boeing 787 (Figure 1) and Airbus A350, already have above 50 % of their structural weight built-in advanced composites (Alemour et al., 2019). On one of the most modern aircraft globally, the F-35 Lightning II, fiber-reinforced polymers are used in load-bearing structures of the aircraft (e.g., vertical stabilizer, tailplane, flaps and wings skin). These components constitute 40 % of the aircraft's weight and are responsible for the aerodynamic lift and maintaining the aircraft in the air. Another advantage is the low detectability by radars this material offers (Bielawski, 2017).

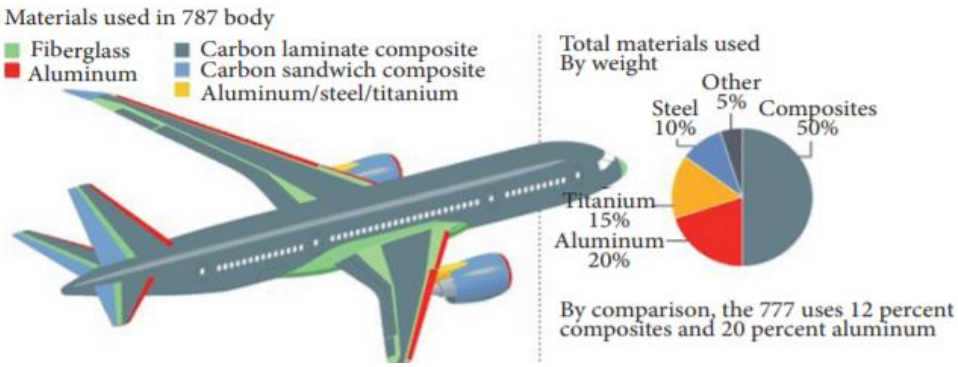

Figure 1- Materials used in the construction of the Boeing 787 (Alemour et al., 2019).

Composite materials are thus becoming a trend in aircraft construction, already being increasingly used in modern civil and military aircraft but also in Unmanned Aircraft Vehicles (UAVs) (Bielawski, 2017). Following this trend, Portugal keeps up with the rest of NATO's state members and has acquired UAVs for all three branches of the Portuguese Armed Forces and qualified personnel to fly them.

The UAVs acquired by the Portuguese military branches are used in different missions and need to be reliable and adapt to different environments. In parallel with the operation of these commercial UAVs, the Portuguese Air Force, through the Investigation Center of the Portuguese Air Force Academy (CIAFA), has been developing research in the conception (project), construction and optimization of their own UAVs, with specific characteristics adapted to their missions. Although CIAFA uses carbon-fiber-reinforced composites as one of the primary materials in the fabrication of UAVs, even so it is crucial to find new ways to reduce weight and improve the strength of the components of these unmanned aircraft (Soares, 2021).

The interest in the effect of radiation on polymer materials grew rapidly with the recognition of the potential of associated techniques to improve their physical-chemical and mechanical properties and as a testing parameter for aerospatial applications. Industries like aerospace and electronics require polymers with a specific response when exposed to radiation. Radiation-induced crosslinking and highly durable materials under radiation fields are some properties these industries are looking for when designing and developing these materials for high-demanding applications (Reichmanis et al., 1993).

Fiber-reinforced composite materials are usually cured at room temperature or with heat, but the radiation-assisted cure can significantly improve strength, curing time and process cost. In addition, the radiation-assisted cure improves the composite through polymerization and crosslinking (Cleland et al., 2003).

The suggestions for future work in (Soares, 2021) motivated this dissertation, namely the suggestion to study the effect of the radiation-assisted cure in the preparation of the carbon-fiber-based composites commonly used in CIAFA. In addition, the curing process will be revised to allow the preparation of more homogenous and sturdier material.

1.2. Objectives

This study aims to assess whether it is possible to improve carbon-epoxy composites' mechanical and thermal properties, with potential application in aeronautics, through controlled exposition to gamma radiation. The main goal is to evaluate how the radiation-assisted cure influences the treated material's final properties compared to post-cure irradiation. To accomplish this, the material was subjected to gamma irradiation in different stages of the resin's cure, and the respective thermal resistance and mechanical behavior were exhaustively evaluated.

1.3. Dissertation Layout

Chapter 1.

This chapter briefly introduces the use of composite materials in civil and military aviation, followed by the motivation to study the impact of radiation-assisted cure in carbon-epoxy composites and the dissertation objectives. The dissertation structure is presented and specified at the end of the chapter.

Chapter 2.

This chapter gathers the theoretical basis of the work presented in this dissertation. It includes the definition of fiber-reinforced composites, their characteristics, applications, mechanical and thermal properties, and the effects of gamma radiation on polymer-based materials.

Chapter 3.

This chapter describes the method and the materials used to fabricate the carbon-epoxy test specimens. In addition, the irradiation process and the three irradiation methodologies followed are explained. Finally, the chapter ends with a description of the mechanical and thermal analysis characterization of the materials prepared.

Chapter 4.

This chapter presents the data obtained from the preliminary study and the mechanical and thermal analysis characterization. In addition, the experimental data from tensile, flexural, thermogravimetric analysis and differential scanning calorimetry are reviewed in detail.

Chapter 5.

In this last chapter, the results obtained in each radiation methodology are summarized and compared in a correlational way. Furthermore, the limitations of this work are presented, and some recommendations for future work are given.

2 Literature Review

2.1. Fiber Reinforced Composites

Fiber-reinforced polymer composites consist of high strength and modulus fibers combined with a polymer-based matrix (Figure 2). Both fibers and matrix have very different physical and chemical identities. However, when combined, they attain properties that the individual components can not attain alone. In general, fibers are the principal load-carrying members and the surrounding matrix keeps them in the desired position and orientation, acting as a load transfer mechanism between them. The matrix also protects the fibers from the environment, such as elevated temperatures, humidity and aggressive agents (oxidants, fuel lubricating greases, etc.) (Mallick, 2007).

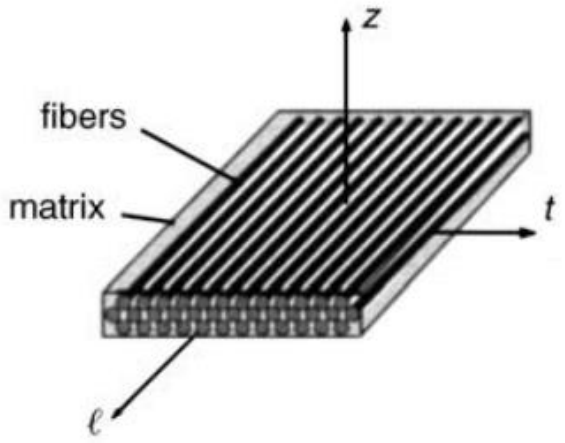

Figure 2 - Composite constitution (fibers + matrix) (Gay et al., 2002).

The most common form of fiber-reinforced composites in structural applications is called laminate. A laminate consists of series of stacked layers of fibers and matrix, consolidated in the desired thickness. Fiber orientation in each layer and the stacking sequence of different layers in the laminate can be changed to create a range of different physical and mechanical properties (Mallick, 2007). In the case of carbon fiber, each layer or lamina has thousands of fibers along its thickness because each fiber tow comprises thousands of carbon filaments (Chung, 2010).

2.1.1. General Characteristics

Most fiber-reinforced polymers offer a combination of strength and modulus comparable to or better than most traditional metallic materials. In addition, because of their low density, the strength-to-weight ratios and modulus-to-weight ratios of these composites are significantly superior to those of metals. For these reasons, fiber-reinforced polymers have become a

significant class of structural materials and are being used, or considered for use, as replacements for metals in many weight-critical components in the aerospace, automotive, and other industries. (Mallick, 2007).

Metals, such as steel and aluminum alloys, are considered isotropic because they exhibit nearly the same properties regardless of load direction. On the other hand, fiber-reinforced composite materials can be very heterogeneous and anisotropic. In addition, these materials are typically designed for a specific application by arranging the fibers according to the loading condition, making it possible to attain an optimized load-bearing capacity while saving additional weight (Gay et al., 2003).

2.1.2. Applications

The number of applications for fiber-reinforced polymer composites is vast, making it difficult to quantify. So instead, this section highlights the major structural applications in aerospace for composite materials. Currently, aircraft already have many components made of composite materials (e.g., primary structure components, control surfaces, exterior and interior components). Some examples are shown in figures 3 and 4 (Gay et al., 2003):

Figure 3 - F16 Radome (General Dynamics to Build Wide-Band Radomes for F-16s | Shephard, n.d.).

Figure 4 - Boeing 787 : Composite civil aircraft (Boeing: 787 Dreamliner, n.d.).

Fiber-reinforced polymer composites are also used in other areas such as sporting goods (e.g., fishing poles, skis, surfboards and bicycle frames), electronics (e.g., antennas and windmills), buildings and public works (e.g., chimneys, concrete molds, doors and furniture), road transports (e.g., chassis, suspension springs and transmission shafts), marine transports (e.g., canoes and racing boats) (Gay et al., 2003).

2.1.2.1. Aircraft and military applications

Even though fiber-reinforced composites have countless applications, they are primarily used in aircraft and military applications for their low density to stiffness ratio and flexible

design, leading to a significant weight reduction, which is critical for increasing speeds and payloads. Boron fiber-reinforced epoxy skins were first used for the F-14 horizontal stabilizers in 1969. With the introduction of carbon fibers in the 1970s, carbon fiber-reinforced composites became the primary material in wings, fuselages and empennage components (Figures 5 and 6). These components proved their integrity and durability through the years, building up confidence in composites, which led to the development of other structural components, increasing the number of composite parts used in military aircraft today. Weight reduction is essential for military aircraft. However, the use of carbon fibers, special coatings, and design features also reduces radar reflection and heat radiation contributing to the stealth characteristics of military aircraft (Mallick, 2007).

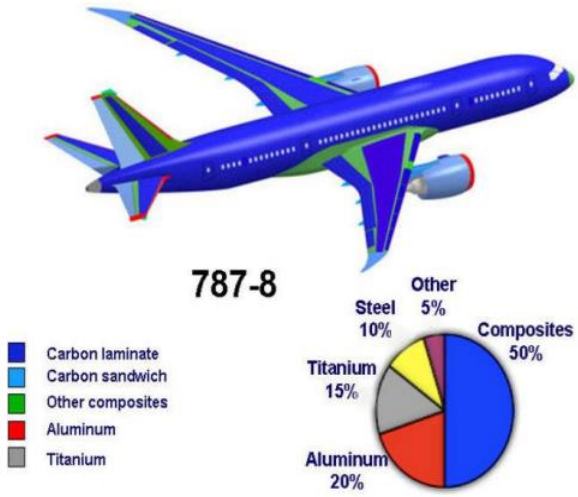

Figure 5 - Materials used in Boeing 787- 8 (Smith, 2013).

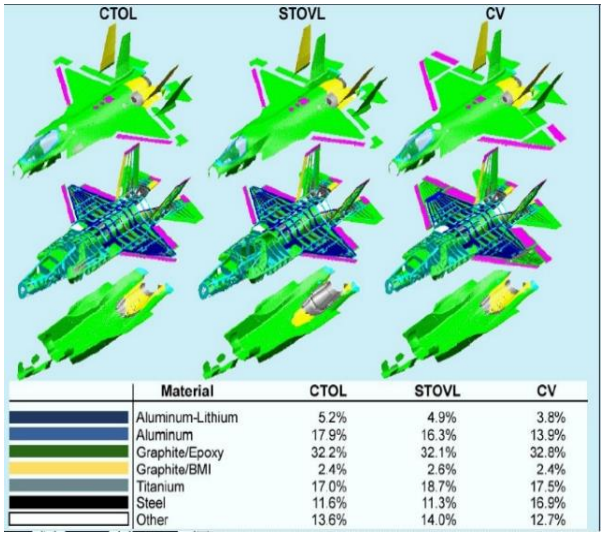

Material	CTOL	STOVL	CV
Aluminum-Lithium	5.2%	4.9%	3.8%
Aluminum	17.9%	16.3%	13.9%
Graphite/Epoxy	32.2%	32.1%	32.8%
Graphite/BMI	2.4%	2.6%	2.4%
Titanium	17.0%	18.7%	17.5%
Steel	11.6%	11.3%	16.9%
Other	13.6%	14.0%	12.7%

Figure 6 – Material composition of the Lockheed Martin F35 JSF (Loyola, 2014).

Carbon-fiber reinforced composites are heavily used in military aircraft, helicopters and UAVs. It is foreseen that by the end of 2025, the carbon-fiber-reinforced composites in the aerospace and defense industry will reach 1.56 billion dollars, and the UAV aircraft's value will grow exponentially until the end of that year (Figure 7) (Yadav et al., 2021).

Lightweight and high-strength carbon-fiber-reinforced composites manufactured by the vacuum bag technique allow the overall UAV's weight to be reduced by 15 to 45 %, depending on the percentage of composite used in the structure (Yadav et al., 2021).

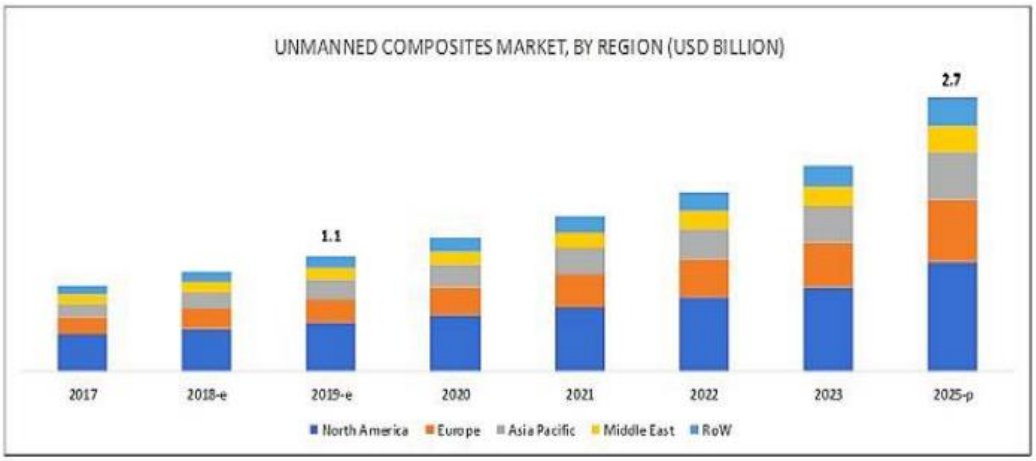

Figure 7 - Unmanned composites market, by region (Yadav et al., 2021).

2.1.3. Fibers

Fibers consist of thousands of filaments with a diameter of 5 to 15 micrometers which allows them to be produced using textile machines. Short fibers are used in injection molding and to produce felts and mats. Long fibers are normally used to fabricate wovens that are then cut to fabricate composite materials. The principal fiber materials used for composite preparation are glass, aramid, carbon, boron and silicon carbide (Gay et al., 2003). These fibers are bundled together in tows which are identified according to the number of filaments they contain. Common tow ratings are 3K, 6K, 12K and 15K. The K refers to a thousand, so a 3k tow is made with 3000 filaments (Latteier, 2019).

The use of fibers as a reinforcement for cold-setting resins has long been used in the electrical area because of its insolation properties. But, the first synthetic fiber used as a reinforcement to produce a composite material with high strength, stiffness and low relative density was glass fiber. Currently, there are a lot more synthetic fibers such as carbon, boron and ceramics that can produce a material with such properties. Nevertheless, research continues with the objective of producing materials with an increasing strength-to-weight ratio, especially in the aerospace industry (Bolton & Higgins, 2014).

The fibers used to fabricate laminates can be arranged in a unidirectional orientation (Figure 8 type 1 and 2), a bidirectional orientation (Figure 8 type 3) or a multidirectional orientation (Figure 8 type 4). The last two fiber orientations are obtained normally through weaving. For unidirectional fibers, the strength and modulus reach their maximum values in the longitudinal direction of the fiber. However, these values decrease greatly in the transverse direction. Bidirectional fibers can vary their properties by using different amounts of fibers for each direction. However, an equal distribution of the fibers provides equal properties in both

directions. Also, each laminate's layer may have the fibers oriented in one direction or in different directions (Mallick, 2007).

Type	Fiber Architecture		Remarks
1	Unidirectional one layer		N/A
2	Unidirectional two layers		N/A
3	Bi-directional		Bi-directional one layer
		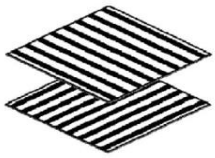	Bi-directional using 0°/90° unidirectional fibers (two layers)
4	Random		Chopped fibers (25-75 mm) placed randomly in matrix

Note: N/A is not available

Figure 8 - Fiber orientation in fiber-reinforced composites (Khoe et al., 2011).

The carbon fabrics are made of fibers oriented along two perpendicular directions. One is called warp, and the other is called fill (or weft). The fibers are woven together so that the fill yarns pass over and under the warp yarns, following a constant pattern. The stiffness obtained with a woven fabric is less than if two cross plies of unidirectional fibers are superposed because of the curvature the fibers acquire after weaving (Figure 9). Figure 10 represents a plain weave pattern (Gay et al., 2003):

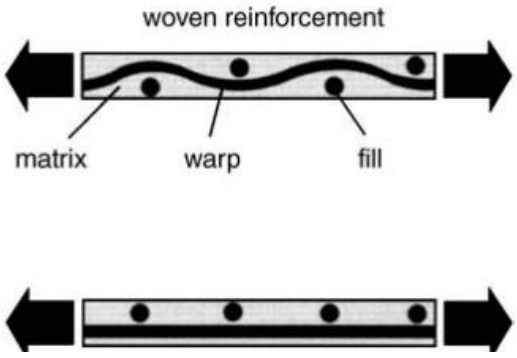

Figure 9 – Cross-section of a layer with fibers crossed at 90° (Gay et al., 2003).

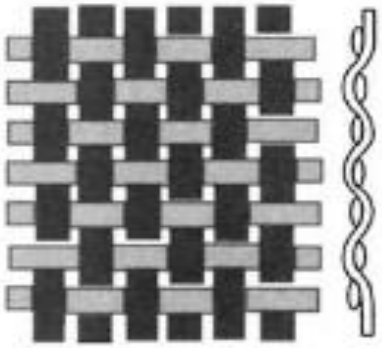

Figure 10 - Plain weave pattern, adapted from (Gay et al., 2003).

Carbon Fiber

Carbon fiber's advantages are their exceptionally high tensile strength to weight ratio and tensile modulus to weight ratio, low coefficient of thermal expansion, fatigue strength, and high thermal conductivity. On the other hand, their low failure strain and low impact resistance are disadvantages. In addition, high costs exclude carbon fibers from most commercial applications; they are mostly used in the aerospace industry since weight saving is more important than cost or in industries where cost is a secondary problem (Mallick, 2007).

Carbon fiber is made of layers of carbon atoms arranged in a structure similar to graphite, but instead of small "plates" of atoms that slide over each other, carbon fiber forms long fibers. Strong covalent bonds unite the atoms along a layer; weak van der Waals forces connect each layer. As a result, carbon fiber is anisotropic in most of its properties (Bolton & Higgins, 2014).

2.1.4. Matrix

The matrix purpose in a composite material is to keep the fibers in place, transfer the stress to the fibers, provide a barrier against the environment, and protect the fibers' surface from mechanical degradation. The matrix influence on the tensile load-carrying capacity is minor on a composite, but it is important to provide lateral support to the fibers and avoid buckling under compressive loads (Mallick, 2007).

Some examples of lightweight matrices include polymers, carbon, ceramics and metals. These matrices have a wide spectrum of temperature capabilities, so the matrix's choice often depends on the composite's temperature requirement. For example, carbon and ceramic are used for high-temperature applications, metal matrices for moderately high temperatures and polymer for applications that do not involve high temperatures (Chung, 2010).

Polymer matrices can be divided into two groups, thermosetting and thermoplastic polymers. Thermoplastic polymers lose their rigidity when subjected to heat, which allows them to be reshaped under pressure, maintaining the new shape after cooling. On the other hand, thermosetting substances become permanently rigid after the molding process because they suffer permanent chemical changes that can not be reversible (Bolton & Higgins, 2014). This happens because thermoplastic polymers are held in place by weak van der Waals bonds and hydrogen bonds that can be temporarily broken with heat. On the other hand, in a thermoset polymer, the molecules are chemically joined by crosslinks, formed during polymerization, creating a three-dimensional network structure (Mallick, 2007). Figure 11 represents the thermoplastic and thermoset polymers:

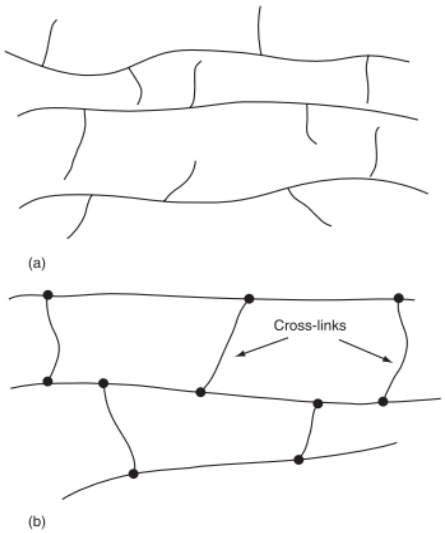

Figure 11 - Schematic representation of (a) thermoplastic and (b) thermoset polymers (Mallick, 2007).

Epoxy Resin

Epoxy is the most used polymer matrix for structural applications because of its strong adhesiveness with different fibers, excellent mechanical properties, corrosion resistance, stability, and relatively low price. Also, uncured epoxy has a relatively low molecular weight in the liquid state resulting in high molecular mobility during composite fabrication. This mobility helps during the fabrication process since the resin can quickly spread and impregnate through the carbon fibers (Chung, 2010).

Epoxy cures when mixed with a catalyst. This process consists of a reaction that involves crosslinking (Chung, 2010). Curing is initiated by adding a curing agent and as the curing progresses, molecules start crosslinking, forming a three-dimensional structure resulting in a solid epoxy matrix (Figure 12) (Mallick, 2007).

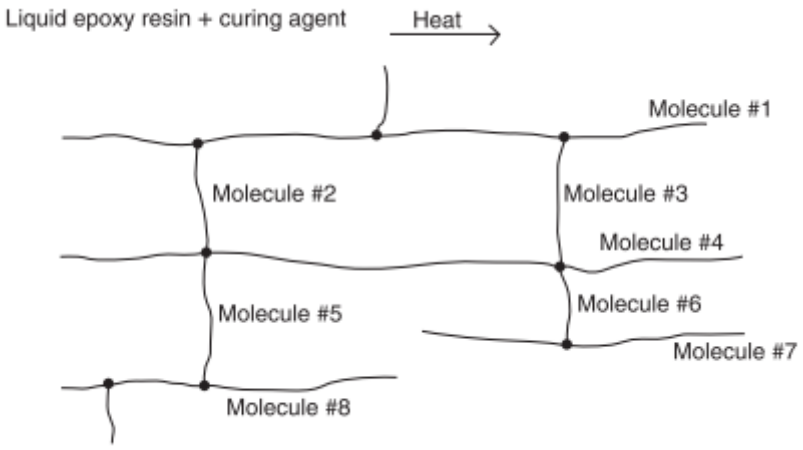

Figure 12 - Fully cured epoxy resin (Mallick, 2007).

The cured epoxy matrix's final properties will depend on the crosslinking density. Generally, higher crosslinking improves tensile modulus, glass transition temperature, thermal stability, and a consequent decrease in elongation at break (Mallick, 2007).

2.2. Material Properties

2.2.1. Mechanical Properties

Structural applications require mechanical properties (e.g., strength and stiffness) in the material to bear the load in the structure. In addition to mechanical properties, a structural material may be required to have other properties, such as low density to save fuel in the case of aircraft and corrosion resistance for the durability of all structures. Mechanical performance is fundamental to the selection of structural material. Strength, modulus and ductility can be measured in tension, compression or bending. Fiber-reinforced polymers are dominant, as structural materials, due to their high strength and low density (Chung, 2010).

The carbon-fiber-reinforced composites properties, such as bending, tension, impact and torsion, are crucial when designing a structure. These properties vary depending on the used fiber and matrix. Carbon-epoxy composites are becoming the most used fiber-reinforced composites because of their excellent mechanical properties and relatively low cost (Deokar & Visal, 2019).

Strain is defined as the change in dimension per unit length. Stress arises when the applied force acts perpendicular to the area of interest. The strain is **elastic** when it fully recovers from applied stress and the material subjected to the stress does not show any permanent deformation. In most materials, the elastic stress-strain relation is linear (Figure 14) and can be expressed by Hooke's law (Wright & Askeland, 2014):

$$\frac{\sigma}{\varepsilon} = E \qquad (1)$$

where σ is the stress in Pascal (Pa), ε is the strain value (m/m), and E is the Young's modulus or modulus of elasticity in Pascal.

Permanent deformation in a material is known as **plastic** strain. After the stress is removed, the material does not return to its original shape. The material's yield strength is the critical stress value that initiates the plastic deformation (Figure 14). The material behaves elastically with stresses below this limit and above, like plastic.

The yield strength corresponds to the intersection of the offset line (usually 0.002 strain offset) and the stress-strain curve. Thus, tensile strength (Figure 13) is the maximum stress on the stress-strain curve, also known as ultimate tensile strength (Wright & Askeland, 2014).

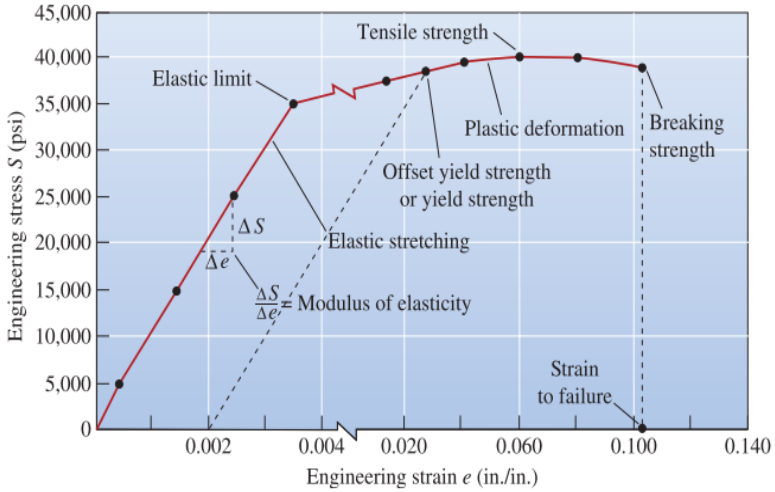

Figure 13- Stress-strain diagram (Wright & Askeland, 2014).

In many materials, tensile tests are sometimes hard to be performed because of superficial flaws. Often, just placing the test specimen in the grips of the tensile machine can cause cracking. An alternative to tensile testing is the bending test. The load is applied at three or four points, causing bending, and a tensile force acts on the test specimen opposite the midpoint causing a fracture. Figure 14 represents the stress-deflection curve of a bending test:

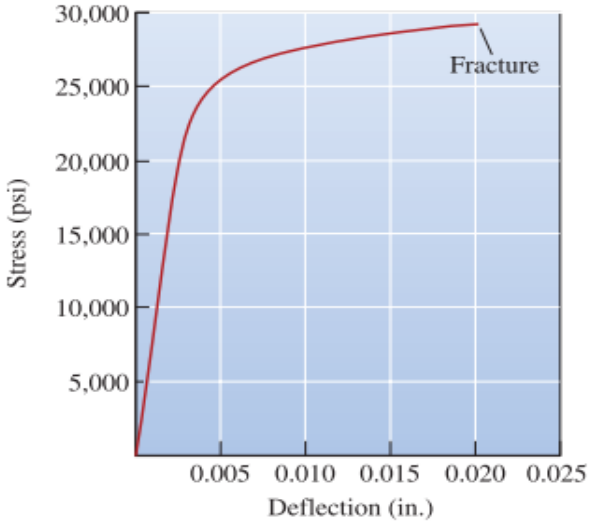

Figure 14 - Stress-deflection curve from a bending test (Wright & Askeland, 2014).

The bending test results are similar to the stress-strain curve, but the stress is plotted with deflection instead of strain (Wright & Askeland, 2014).

2.2.2. Thermal Properties

The inability to tolerate high temperatures is a problem with most polymer-based materials. This inability is related to the degradation of the polymer itself (Chung, 2010).

Glass transition temperature (T_g) and degradation temperature (T_{deg}) are two properties that define the thermal stability of the material's structure. Therefore, improving these properties is the key to improving the structural stability of a composite's matrix regarding its thermal behavior (Rami et al., 2010).

One of the most important properties of polymers is T_g. It describes the temperature region where the mechanical properties of the polymeric material change from hard and brittle to soft and rubber-like. Normally its investigated through Differential Scanning Calorimetry (DSC) analysis (Seifi et al., 2020).

In an amorphous solid, like polymer-based materials, the glass transition temperature is a temperature limit at which the resin softens. The softening at T_g is due to the movement of the constituent molecules, ions or atoms above T_g. Below T_g, there is insufficient thermal energy for such movements to occur. T_g is below the melting temperature (Chung, 2010).

Thermal degradation behavior is a very important property of polymeric materials. It corresponds to a type of polymer degradation where adverse chemical changes (e.g., scission of molecular chains) occur with increasing temperature, without the simultaneous involvement of other compounds such as oxygen. Consequently, polymers may undergo chemical reactions, and small molecular fragments can evolve in gaseous form. Consequently, there is a reduction in the mass of the material and its structural cohesion, negatively impacting the material's structural integrity and robustness (Callister & Rethwisch, 2017).

Normally Thermogravimetric Analysis (TGA) monitors the weight change of a sample inside a furnace, in a controlled atmosphere, with increasing temperature. This technique gives information about the material's thermal stability (Seifi et al., 2020).

Glass transition temperature and thermal degradation temperature are two thermal properties that demonstrate the robustness of polymer-based materials. These properties will be analyzed to characterize the carbon-epoxy composite studied in this dissertation.

2.3. Effects of Gamma Radiation on Polymer-Based Materials

It is possible to modify material's physical, chemical and biological properties by exposing them to ionizing radiation. This process is defined as the radiation processing of materials, which can be controlled and used to develop or alter specific properties of a material.

To understand the irradiation processing of materials, there is the need first to understand basic radiation physics, radiation sources and the interaction between radiation and matter (Sun & Chmielewski, 2017).

2.3.1. Ionizing Radiation

Ionizing radiation designates electromagnetic radiation or accelerated particle beams with enough energy to ionize atoms and molecules which includes α and β particles, electron beams, X-rays and gamma radiation (Ferreira, 2008).

Ionizing radiation can modify the physical and chemical properties of the irradiated material. One of the main industrial applications for radiation is materials modification (polymer crosslinking). Other applications include sterilization of healthcare products and irradiation of food and agriculture products to extend shelf life, disinfestation and pest control (Drobny, 2012).

Ionizing radiation can induce chemical reactions, including polymerization and crosslinking. In the case of radio-polymerization, first occurs the ionization and creation of free radicals on the monomers.Then polymerization is induced through regular radical polymerization of chain initiation, propagation and termination. (Makuuchi & Cheng, 2011). In the case of crosslinking, the modifications are due to the reaction of free radicals produced by the ionizing radiation and the excited species initially produced by irradiation (Sun & Chmielewski, 2017).

2.3.2. Radiation Sources

Radiation can be defined as the emission or transmission of energy in the form of particles or electromagnetic waves through space or through a material medium. The first one includes electrons, positrons, protons, neutrons and ions; the second covers a wide wavelength range, including infrared, visible, ultraviolet radiation, X-rays, and gamma radiation, as shown in Figure 15 (Sun & Chmielewski, 2017).

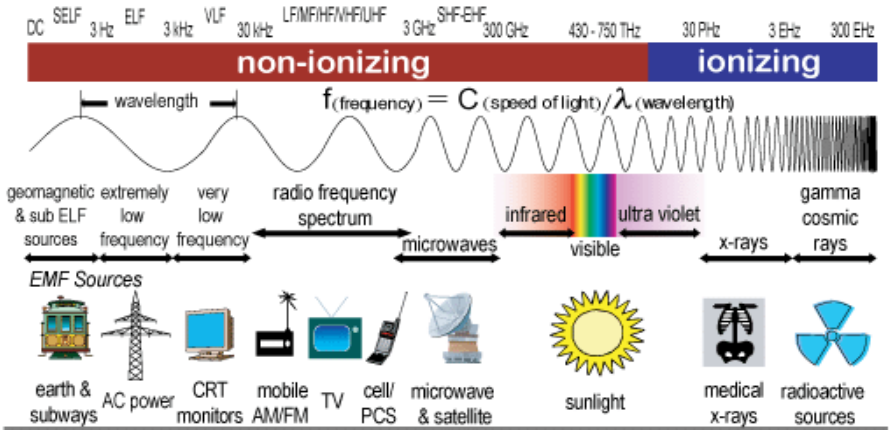

Figure 15 - Electromagnetic radiation spectrum *(Uthman et al., 2020)*.

The primary radiating sources for radiation modification of polymer properties include gamma-radiation from radioactive isotopes such as Cobalt-60, electron beams (E-Beam) from electron accelerators, and X-rays converted from electron beams (Makuuchi & Cheng, 2011).

Radiation from electron beams has low penetration capacity and high dose rates compared with gamma radiation, and due to this, its application in properties modification is mostly reduced to surface treatments and modification of low-density materials. Electron beams typically have energies between 0.2 and 12 MeV (Ferreira, 2008). Compared to gamma-radiation, it shows some advantages since it is a very fast, precise, and clean process. In addition, there is no permanent radiation because it does not use radioactive elements, is almost waste-free, and does not shows any serious environmental hazards (Drobny, 2003).

Gamma-Radiation

Gamma-radiation produced by radioactive decay interacts with matter molecules through secondary electrons as high-energy electromagnetic radiation. The typical energy of gamma-radiation is a few hundred electron volts (eV), higher than the energy of ultraviolet (UV) light and slightly higher than X-rays. Cobalt-60 is the most commonly used radiation source for industrial applications (Makuuchi & Cheng, 2011).

First, cobalt-60 decays into the excited-state nickel-60 isotope, emitting one negative β particle with a half-life of ~ 5.27 years. Then, the excited state nickel-60 further decays into stable nickel-60, emitting two photons with 1.173 and 1.333 MeV, respectively (Figure 16) (Makuuchi & Cheng, 2011).

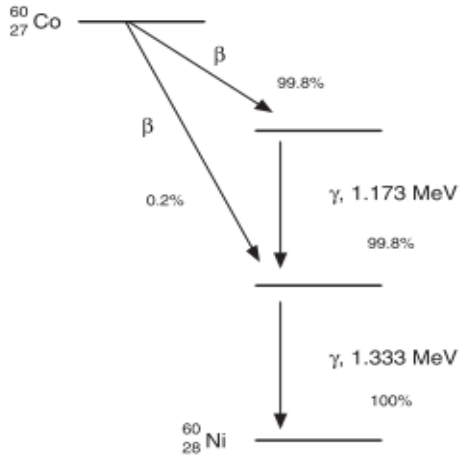

Figure 16 - Radioactive decay of Cobalt-60 (Makuuchi & Cheng, 2011).

The amount of the radioisotope is indicated by the unit for radioactivity, Curie (Ci): 1Ci of a radioisotope disintegrates at $3.7\ x\ 10^{10}/s$. Each cobalt-60 emits a toal of 2.506 MeV per desintegration (Makuuchi & Cheng, 2011).

2.3.3. Units and Dosimetry

In radiation processing, dosimetry measures the energy deposited in the irradiated material. There are different dosimeters for each application, which have different requirements for dose determination (Sun & Chmielewski, 2017). Polymethyl methacrylate (PMMA) dosimeters are among the most used routine dosimeters in gamma radiation processing units (Ferreira, 2008). PMMA dosimeters (Figure 17) were used in this study to measure the absorbed dose of each test specimen.

Figure 17 - PPMA routine dosimeter (Harwell Amber Perspex Dosimeter) (Soares, 2021).

Absorbed dose and the distribution of dose across the material are essential parameters for quality control of the radiation processing of materials. Absorbed dose (D) is the energy absorbed by a substance per unit mass. The SI unit for absorbed dose is Gray (Gy), which equals 1 J/kg. Dosimeters measure the absorbed dose during radiation processing (Makuuchi & Cheng, 2011).

Dose uniformity (U or DU) is another parameter to consider during radiation processing. Dose uniformity is a ratio between the maximum and minimum values of the absorbed dose (D_{max}, D_{min}). The absorbed dose per unit of time is commonly expressed as dose rate, and its unit is $kGy.s^{-1}$ (Ferreira, 2008).

2.3.4. Interaction of Ionizing Radiation with Polymers

When gamma-radiation interacts with a polymer, its energy is absorbed and radicals are produced, initiating various chemical reactions, such as:

- Crosslinking, where polymer chains are connected, formatting a network;
- Chain scission, where the molecular weight of the polymer is reduced.

Crosslinking and chain scission always coexist under radiation, one predominant over the other, depending on the type of polymer (degradative or crosslinking type) (Figure 18).

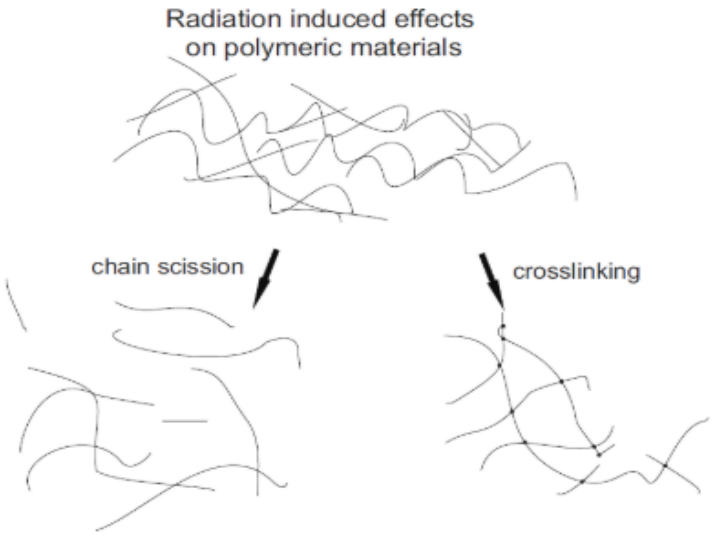

Figure 18 - Crosslinking vs chain scission of a polymeric material (Sun & Chmielewski, 2017).

However, the overall effect depends on which of the two is predominant at a specific time. Typically, crosslinking improves the mechanical and thermal properties of the polymer, reduces the melt flow and increases the viscosity of the polymer solution. In contrast, chain scission deteriorates the mechanical and thermal properties of the polymer (Makuuchi & Cheng, 2011).

Crosslinking is the most important effect on radiation-assisted cure processes, improving the mechanical and thermal properties and the material's chemical, environmental, and radiation stabilities. Crosslinking and chain scission occur during this treatment, but one may be predominant over the other (Cleland et al., 2003).

The radiation-assisted cure is a radiation-chemical process where crosslinking occurs at an earlier stage. Since gamma rays have much higher energy than ultraviolet light, they can penetrate deeper, enabling the curing of much thicker materials such as composites (Makuuchi & Cheng, 2011).

The crystallinity and molecular weight increase due to crosslinking causes an increase in the failure load and Young’s modulus but a decrease in elongation at break because the material becomes stiffer. Since glass transition temperature is related to the free movement of the polymer’s main chains, crosslinking will increase the glass transition temperature due to the high number of covalent chemical bonds formed, which results in a material with less molecular mobility (Sun & Chmielewski, 2017).

3 Experimental Methodology

3.1. Materials

The carbon-fiber/epoxy laminates used for the tensile and flexural test specimens were fabricated according to ISO 527-4/2020 and ISO 14125/2011, respectively. The laminates were fabricated with a 3K carbon mat (Figure 19) with 160 $g.m^{-2,}$ and the tab reinforcements for the tensile testing were made from a 1K carbon mat with 90 $g.m^{-2}$. The reinforcement tabs were added before curing.

The resin used as matrix is a two-component epoxy resin SR8200 with an SD7206 hardener from Sicomin© (Figure 20). According to the manufacturer, this resin achieves a triple purpose: low toxicity, good mechanical properties and low cost. In addition, according to the manufacturer, the glass transition temperature is 50ºC, and the hardener allows unmolding after one night at 20-25ºC, being fully cured after 10 days at 23ºC.

These materials are the ones available and most used at the Investigation Center of the Portuguese Air Force Academy and, for that reason, were the ones used for this thesis. The SR8200 epoxy resin and SD7206 hardener are new at CIAFA because the old resin was discontinued.

Figure 19 - 3K carbon mat used for the laminates.

Figure 20 - SR8200 resin and SD7206 hardener.

3.2. Composite fabrication process

The fabrication process chosen was wet-layup. Firstly a wax layer was applied to the glass mold to prevent the laminate from sticking, which also helps release the laminate faster after the initial 24-hours cure. Next, the two-compound resin was prepared under the manufacturer's instructions adding 27 % (W/W) SD7206 hardener. Then the first carbon layer is placed over the wax and impregnated with the epoxy resin. Subsequently, new layers are then applied and impregnated over each other using a paint roller. On top of the laminates, a perforated released

film is applied as well as a breather cloth. The breather cloth allows air circulation for the vacuum process, and it absorbs excess resin, which helps maintain the uniformity of the composite laminate. Finally, the sealing tape is applied around the laminate to secure the vacuum bag. The vacuum prevents the formation of air bubbles and provides homogeneity to the laminate. Figure 21 shows the wet layup setup used to fabricate the laminates:

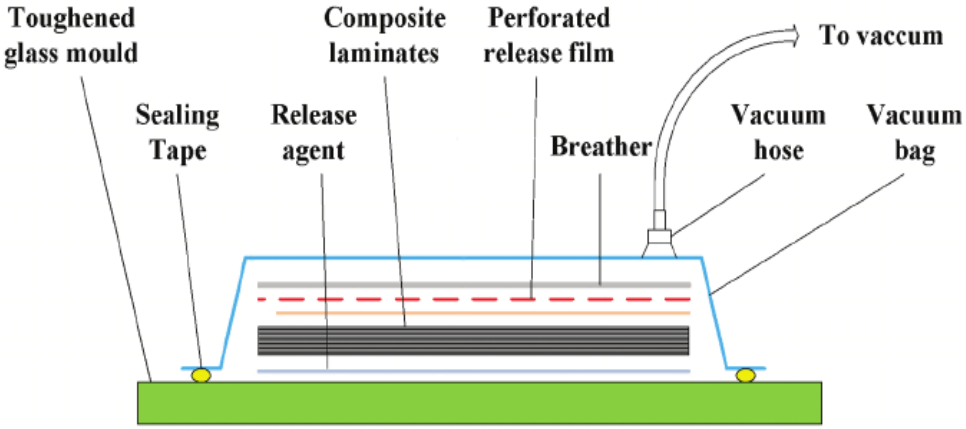

Figure 21 - Wet layup process diagram (adapted from Hang et al., 2015).

Since tensile test specimens require reinforcements for the machine grips, additional layers of carbon were placed and impregnated over the main laminate in specific regions. This step was not necessary for the flexural test specimens. The main laminate required 8 layers of the 160 $g.m^{-2}$ carbon mat for tensile and flexural testing. The reinforcements added to the tensile test specimens required 20 strips of the 90 $g.m^{-2}$ carbon mat (10 layers in each tab).

The laminate stayed in the vacuum bag (Figure 22) for 24 hours under negative 50000 Pascal at an average temperature of 21ºC and 40 % of relative humidity before being unmolded.

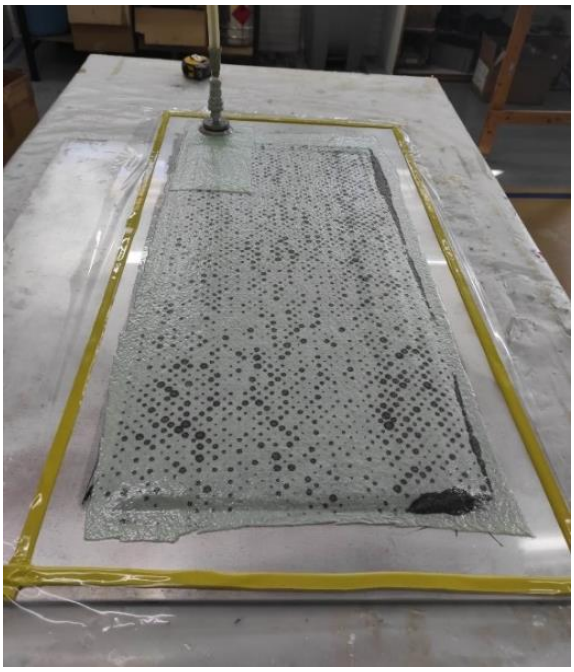

Figure 22 - Laminate curing for 24 hours in the vacuum bag.

A total of 7 panels were fabricated, all with the same dimensions, to cut the tensile test specimens necessary for all the irradiation methodologies. A rule of 40 % fiber and 60 % resin was used to fabricate the panels. Table 1 summarizes the weights of fiber and resin for all the laminates.

Table 1 - Dimensions and weight of laminates for tensile testing.

Irradiation methodology	Laminate	Dimensions [mm]	Fiber [g]	Resin [g]	Total weight [g]	Fiber/Resin [W %]
Post-cure	1	700x300x2	323	425	748	43.18/56.82
	2	700x300x2	331	441	772	42.88/57.12
	3	700x300x2	321	437	758	42.35/57.65
Radiation-assisted cure (2 and 10 days)	4	700x300x2	318	455	773	41.14/58.86
	5	700x300x2	327	473	800	40.88/59.13
	6	700x300x2	329	469	798	41.23/58.77
	7	700x300x2	341	463	804	42.41/57.59

A total of 7 panels were fabricated to cut the flexural test specimens for all the irradiation methodologies. For the first 2 laminates, the dimensions were 320 mmx250 mmx2 mm, and later it was decided to change the dimensions to 350 mm x300 mm x 2 mm for the remaining laminates to increase the distance between each test specimen in the CNC machine. A rule of 40 % fiber and 60 % resin was used to fabricate the panels. Table 2 summarizes the weights of fiber and resin for all the laminates.

Table 2 - Dimensions and weight of laminates for flexural testing.

Irradiation methodology	Laminate	Dimensions [mm]	Fiber [g]	Resin [g]	Total weight [g]	Fiber/Resin [W %]
Post-cure	1	320x250x2	85	121	206	41.26/58.74
	2	320x250x2	92	129	221	41.63/58.37
Radiation-assisted cure (2 and 10 days)	3	350x300x2	159	228	387	41.09/58.91
	5	350x300x2	153	222	375	40.80/59.20
	6	350x300x2	140	190	330	42.42/57.58
	7	350x300x2	146	204	350	41.71/58.29

The dimensions were these because, according to ISO 14125/2011 and ISO 527-1/2020, a minimum of 5 test specimens shall be tested (for tensile and flexural testing). Therefore, to increase the statistical significance of the results, 10 test specimens were fabricated instead of 5 for each dose of gamma radiation studied.

The test specimens were cut using a Computer Numerical Control (CNC) machine (Figure 23). An end-mill of 3,5 mm was installed in the CNC machine and programmed to spin at 2000 RPM. First, the depth of each passage of the end-mill was 0,5 mm, but this required 6 passages in total, which would take approximately 6 hours to cut the entire panel. Next, the passage depth was increased to 1,5 mm to expedite the cutting process, but too many specimens presented imperfections and had to be discarded. So an end-mill passage depth of 1 mm was chosen to cut all the laminates.

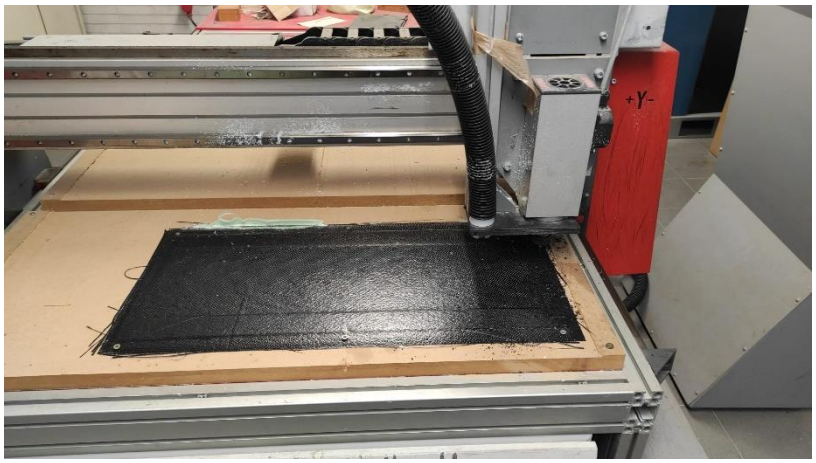

Figure 23 - Laminate ready to be cut in the CNC machine.

Following the cut, all test specimens were sanded with fine-grit (400 grains.cm^{-2}) sandpaper to wipe inconsistencies and give a proper finishing touch to the specimens. Figure 24 represents the laminate excess after CNC cutting has finished. Figure 25 represents two test specimens, one after being removed from the CNC machine (on the right) and the other after being sanded (on the left).

Figure 24 - Laminate after cut and with the test specimens removed.

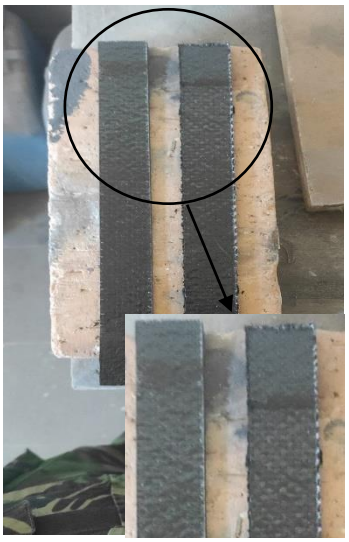

Figure 25 - A finished specimen on the left and a specimen before sanding on the right.

All test specimens were cleaned with isopropyl alcohol and left to dry at room temperature before irradiation. Figure 26 represents some finished and cleaned flexural test specimens ready for irradiation.

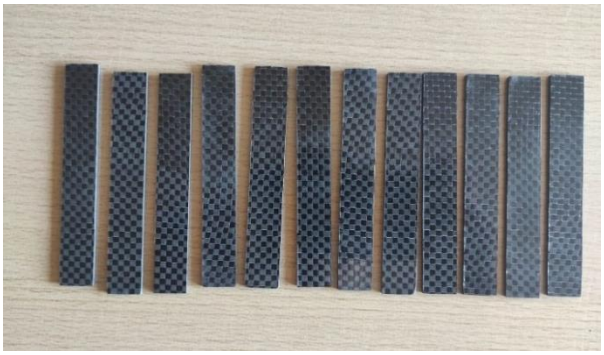

Figure 26 - Flexural test specimens after isopropyl alcohol cleaning.

3.3. Irradiation process

Irradiations were conducted in an experimental Cobalt-60 gamma irradiator PRECISA 22 (Figure 27) at the Ionizing Radiation Facilities laboratory (IRIS) managed by the Radiation, Elements and Isotopes Research Group (GREI) of the Center For Nuclear Sciences And Technologies (C^2TN), (*Instituto Superior Técnico, Universidade de Lisboa*). Samples were irradiated under a nitrogen atmosphere at an average dose rate of 0,4 $kGy.h^{-1}$. The irradiator has four sources of Cobalt-60 for a total of 1.5 kCi measured on the 1st of November 2021.

The preliminary study regarding dose distribution done by (Soares, 2021) was used as a reference for the work developed in this thesis since the radiation geometry was identical and the dose uniformity (U) results obtained were close to 1. Equation 2 shows how the dose uniformity is calculated:

$$U = \frac{D_{max}}{D_{min}} \qquad (2)$$

Dmax is the maximum dose registered, and Dmin is the minimum dose registered in the irradiated total volume.

Figure 27 - Precisa 22 cobalt-60 gamma irradiator.

Figure 28 represents the irradiation supports designed by Soares (2021). Figure 29 represents the irradiation support inside the irradiation chamber of PRECISA 22 cobalt-60 gamma irradiator.

Figure 28 - Irradiation supports designed by Soares (2021).

Figure 29 - Irradiation support inside irradiator chamber.

Before irradiation, the specimens were put in a sealable plastic bag. Firstly the bags were previously deaerated with nitrogen and then evacuated with the aid of a vacuum pump and heat-sealed (Figure 30) to guarantee the irradiation happened without oxygen present to avoid materials oxidation. Then the bags were sent for irradiation (Figure 31).

Figure 30 - Air being removed from the plastic bag.

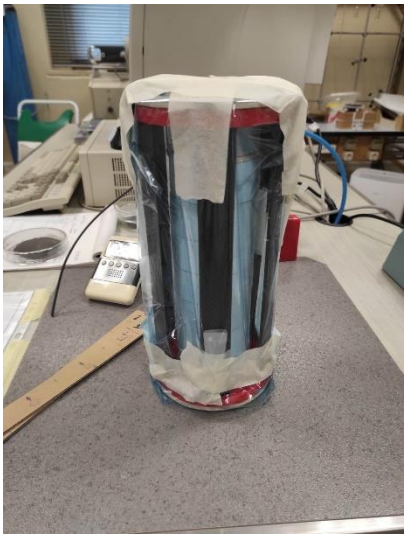

Figure 31 - Irradiation support sealed in the vacuum bag.

3.3.1. Irradiation methodologies

A preliminary study was conducted to assess the optimal doses of gamma radiation regarding its effect on the temperature of degradation of the prepared composite. This study was performed through thermogravimetric analysis of composite samples fully cured and irradiated with doses of gamma radiation from 1.5 kGy to 10 kGy.

The dose range at which a significant improvement in composite degradation temperature was observed was selected to test the composite specimens under 3 irradiation methodologies:

i) Post-cure irradiation, where the specimens were irradiated after the resin is fully cured (≥ 25 days);
ii) Irradiation after 2 days of curing;
iii) Irradiation after 10 days of curing.

The cure schedule of the SR8200 resin with SD7206 hardener is 24 hours under vacuum plus 10 days at room temperature. Figure 32 states the irradiation timeline for each methodology; the common processes between the methodologies are represented in black.

On the one hand, exposing the material to radiation at the beginning of the curing process might improve crosslinking since the curing reaction is fed with additional energy. However, on the other hand, the polymeric chains just started forming and do not provide higher robustness to the polymeric matrix of the composite. Therefore, the radiation might compete with the hardener, increasing the scission effect of the new crosslinked chains instead. Another point of view is that irradiating a fully cured composite might not be as efficient since the matrix is solidified and has lost molecular mobility, making the creation of new crosslinks more difficult.

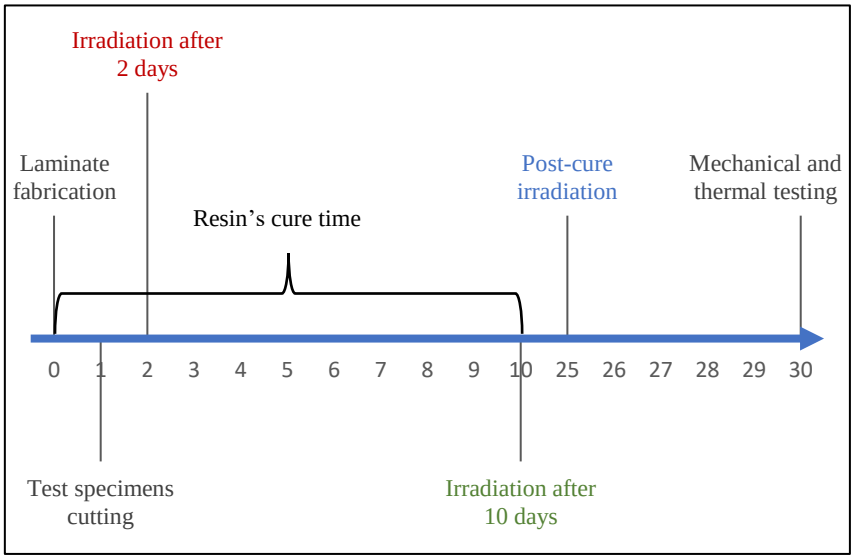

Figure 32 - Irradiation timeline for three different irradiation methodologies.

3.4. Mechanical properties

Testing the materials' properties under different loads allows the observation of their mechanical behavior, specifically, the relation between the applied force and the resulting deformation and the maximum stress which causes the material to fail. A precise characterization of the mechanical properties of materials can be made through a range of standardized testing methods, such as tensile and bending testing. The values obtained from these testing methods are used for materials development, component design, and quality assurance (Groeneveld & Elsea, 2009).

When designing a structure or machine, the effects of force application on materials must be known before manufacturing it. Therefore, numerous mechanical tests have been created to determine such effects over the years. The complete information about these tests' procedures and the materials' behavior when subjected to these tests is specified by American and International standards. In the United States, they are handled by the American Society for Testing Materials (ASTM); and internationally by the International Organization for Standardization (ISO). Based on these standardized tests and values by these organizations, a material can be accepted for a specific application (Bolton & Higgins, 2014).

The tensile test is the most important destructive testing method in materials testing (Groeneveld & Elsea, 2009). Testing the tensile properties of materials involves gripping the test specimens with a known cross-section area in the jaws of a testing machine (Figure 33) and putting it through a constant tensile force; the amount by which the test section length (gauge length in Figure 34) increases is measured for each force increment. This process will continue until the test specimen fails (Bolton & Higgins, 2014). The results of tensile tests are regularly used to ensure quality control; tensile properties are also important in developing new materials and processes to be compared to already existing materials (ASM International, 2004).

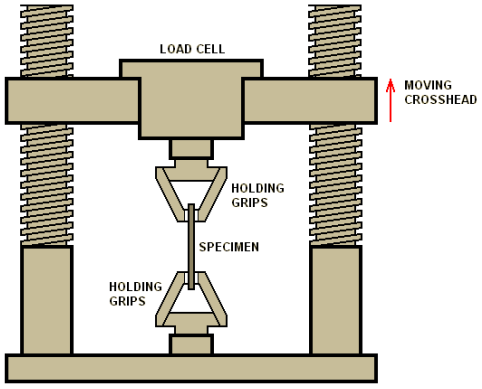

Figure 33 - Tensile testing machine diagram (Sy, 2015).

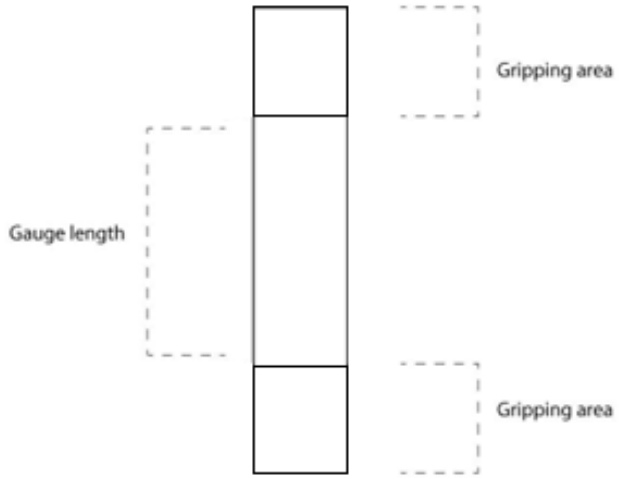

Figure 34 - Gauge length of a test specimen (adapted from Instron, n.d.).

The most frequently studied bending load in materials is the three-point bending test. In this method, a test specimen supported as a beam is deflected at a constant rate until it fractures, demonstrating the relationship between a load and its elastic deformation (Groeneveld & Elsea, 2009). In addition, flexural properties are useful for quality control and specification purposes of unreinforced and reinforced plastics, such as high-modulus composites (ASTM International, 2002). Figure 35 represents the three-point testing method:

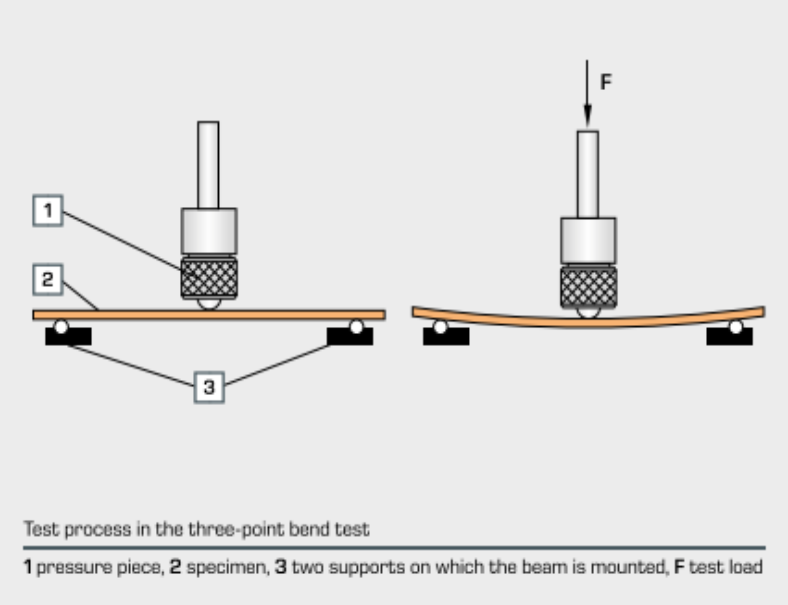

Figure 35 - Flexural testing diagram (Groeneveld & Elsea, 2009).

3.4.1. Tensile testing

Tensile testing was performed on an Instron model 3369 (Figure 36), a universal testing machine with all the requirements of ISO 527-4/2020 - Plastics - Determination of tensile properties - Test conditions for isotropic and orthotropic fibre-reinforced plastic composites. The machine was located at *Laboratório de Mecânica Experimental* (LME) from the *Departmento de Engenharia Mecânica* of the *Instituto Superior Técnico*. It had a load cell of 50 kN installed, and the tests were performed at room temperature (15 to 20 °C) and 40 % relative humidity. The test speed was set to 2 $mm.min^{-1}$ according to ISO 527-4/2020, and data was collected at a frequency of 20Hz. The grips were manually closed, applying enough force on the test specimens to prevent them from slipping out of the grips during the test. In addition, each test specimen was vertically aligned with the grips to prevent any bending or forces applied off-axis.

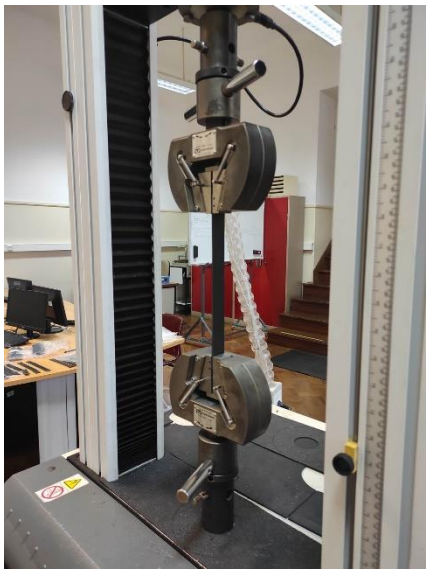

Figure 36 - Instron model 3369 with a 50kN load cell installed.

The testing machine recorded the load and displacement values for each test specimen. With these values, stress, nominal strain and Young's modulus were calculated according to ISO 527-1/2020. Equation 3 was used to calculate stress:

$$\sigma = \frac{F}{A} \tag{3}$$

where σ is the value of stress expressed in megapascal (MPa), F is the measured force in Newton (N), and A is the initial cross-sectional area of the test specimen expressed in square millimeters (mm^2).

Nominal strain is calculated when no extensometer is used, and it was calculated according to Equation 4:

$$\varepsilon = \frac{L_t}{L} \tag{4}$$

where ε is the nominal strain expressed as a dimensionless ratio or percentage; L_t is the gripping distance (gauge length) in millimeters (mm), and L is the increase of the gripping distance (displacement) in millimeters.

ISO 527-1/2020 states that the strain values used to calculate Young's modulus (E_t) must be ε_1 = 0,0005 and ε_2 = 0,0025, but in our case these values did not allow a correct calculation of E_t since the machine was still in an adjusting process at those values (Figure 37). Instead, Young's modulus was calculated using Equation 5:

$$E_t = \frac{\sigma_2 - \sigma_1}{\varepsilon_2 - \varepsilon_1} \tag{5}$$

where E_t is Young's modulus expressed in megapascal; σ_1 is the stress expressed in megapascal, measured at the strain value ε_1 = 0,015; σ_2 is the stress expressed in megapascal, measured at the strain value ε_2 = 0,020.

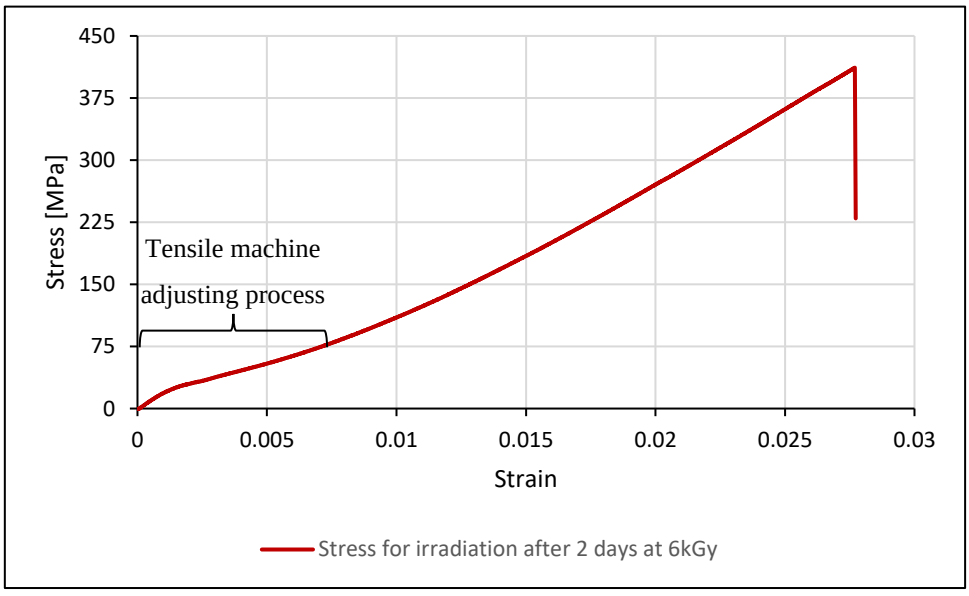

Figure 37 - Stress-strain curve for irradiation after 2 days at 6 kGy.

3.4.2. Flexural testing

Flexural testing was performed on an Instron model 5566 (Figure 38), a universal testing machine. The machine was located at *Laboratório de Ensaios Mecânicos* e de Materiais from the *Departamento de Engenharia Mecânica* of the *Instituto Superior Técnico*. It had a load cell of 500N installed, and the tests were performed at room temperature and 40 % relative humidity. The test speed was set to 2 $mm.min^{-1}$ according to ISO 14125/2011 specifications, and data was collected at a frequency of 50Hz. The span (L) between the two supports is 80 mm, and their radius respects the values stated in the norm.

Figure 38 - Instron model 5566 with a 500 N load cell installed.

The testing machine recorded the load and displacement values for each test specimen. With these values, flexural stress, nominal strain and flexural modulus were calculated according to ISO 14125/2011. Equation 6 was used to calculate flexural stress:

$$\sigma_f = \frac{3FL}{2bh^2} \tag{6}$$

where σ_f is the flexural stress in megapascal; F is the load in Newton; L is the span in millimeters; h is the thickness of the specimen in millimeters, and b is the width of the specimen in millimeters.

The strain in the outer surface of the specimen was calculated according to Equation 7:

$$\varepsilon = \frac{6sh}{L^2} \tag{7}$$

where ε is the strain expressed as a dimensionless ratio or percentage; s is the displacement in millimeters; h is the thickness of the specimen in millimeters, and L is the span in millimeters.

For the flexural modulus, the deflections s' and s" must be calculated according to Equation 8:

$$s' = \frac{\varepsilon_f' L^2}{6h} \; and \; s'' = \frac{\varepsilon_f'' L^2}{6h} \tag{8}$$

where s' and s'' are the beam mid-point deflections in millimeters; ε_f' and ε_f'' are the flexural strains where ε_f'= 0,005 and ε_f''=0,0025.

The flexural modulus is then calculated according to Equation 9:

$$E_f = \frac{L^3}{4bh^3}\left(\frac{\Delta F}{\Delta s}\right) \tag{9}$$

where E_f is the flexural modulus expressed in megapascal; Δs is the difference in deflection between s'' and s', and ΔF is the difference in load F'' and the load F' at s'' and s', respectively.

3.5. Thermal Analysis

Thermal analysis (TA) is a branch of materials science that studies how materials' properties vary as temperature changes. The objective is to establish a connection between temperature and the materials' physical properties. Differential Scanning Calorimetry (DSC) and Thermogravimetric Analysis (TGA) are two of the most popular TA techniques. TA measures the materials' physical properties as a function of temperature and understands their mechanical and thermal histories necessary for materials development, components design, and quality control. Polymers represent one of the main areas where TA is used. (Menczel, Prime, et al., 2009).

3.5.1. Thermogravimetric Analysis

TGA is a technique in which the mass of a material sample is monitored as a function of time or temperature, in a controlled atmosphere, according to a defined heating program in a controlled atmosphere. TGA technique is very popular in polymer research, particularly to study the thermal stability of polymeric systems under application conditions. The mass loss of a polymer-based characterized by TGA helps understand the material's composition, the extent of cure, thermal stability and its degradation kinetic (Menczel & Bruce Prime, 2008).

The thermobalance is the most important part of the TGA, encompassing the reference and working thermocouples and the sampling plate. Figure 39 (a) represents the typical instrumentation of a TGA module, and Figure 39 (b) represents the typical location of thermocouples in the side-loading configuration (Menczel & Bruce Prime, 2008).

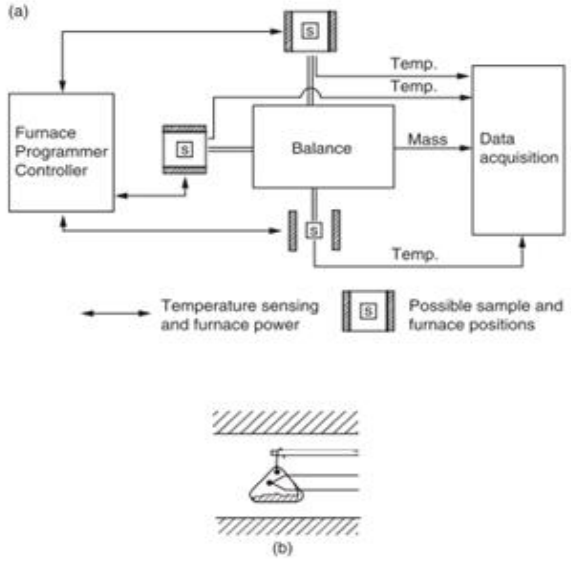

Figure 39 - (a) TGA components in a thermobalance; (b) typical position of thermocouples for side-loading configuration (adapted from Menczel & Bruce Prime, 2008).

Testing was conducted on a TA Instruments model TGA 951 with a nitrogen (N_2) flow of 60 ml.min^{-1}. The samples necessary for each TGA run were collected from at least 5 different test specimens (used for mechanical tests) with the help of a side cutter and mixed to create a single sample. Subsequently, part of the sample (between 7 and 15 mg) was placed on the platinum plate (Figures 40 and 41), and the weight, temperature and relative humidity were registered. All thermal runs departed from room temperature (approx. 21 ºC). The heating program used was:

1. Equilibrate at 30ºC
2. Ramp 10 ºC.min^{-1} to 800ºC

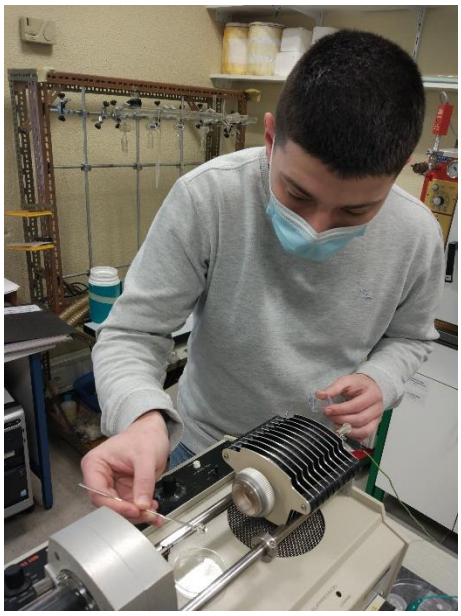

Figure 40 - Sampled being placed in the platinum dish.

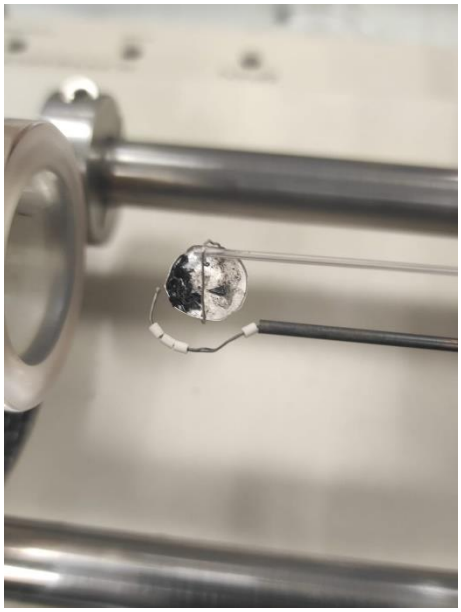

Figure 41 - Platinum plate with sample placed in the thermobalance arm.

3.5.2. Differential Scanning Calorimetry

DSC, just like TGA, is the most popular TA technique. DSC implies that comparative calorimetric information can be obtained on the sample during a linear temperature ramp. One of the major applications of the DSC technique is in the polymer field because of the easy and fast determination of the glass transition temperature, melting and crystallization temperatures, melting enthalpy, heat capacity and thermal history (Menczel, Judovits, et al., 2009). Figure 42 represents a diagram of a DSC instrument:

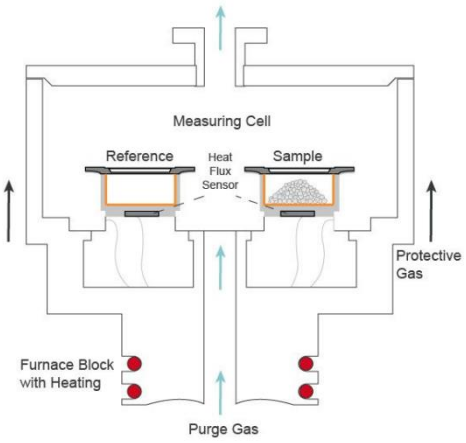

Figure 42 - Diagram of a heat flux differential scanning calorimeter (DSC).

For this work, the samples analyzed by DSC were collected from the test specimens used for the mechanical testing assays. The DSC was used to determine the glass transition temperature, T_g, of the epoxy resin used in the laminate. Since DSC is a destructive testing method, the samples tested were not reusable.

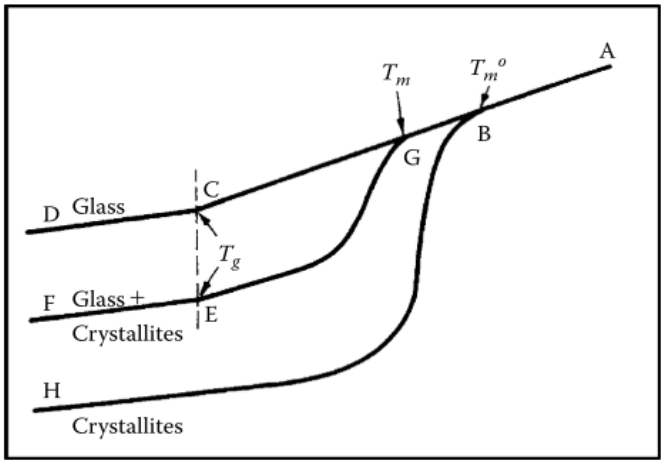

Figure 43 - Representation of the change of specific volume of a polymer at temperature T (Cowie & Arrighi, 2007).

At sufficiently low temperatures, all polymers are rigid solids. However, with increasing temperatures, the polymer obtains enough thermal energy to have its chains moving freely enough to behave like a viscous liquid (if no degradation occurs). An amorphous polymer, whose chains are arranged randomly, follows the curve A-D in Figure 43. Between C-D ($T < T_g$), the polymer behaves like glass, but as it is heated and the temperature becomes higher than T_g, it softens and starts behaving like rubber. T_g represents the material's ability to be deformed more easily (more ductile). Finally, the polymer will start behaving like a viscous liquid for even higher temperatures, increasing Young's modulus loss (Cowie & Arrighi, 2007).

In this work, tests were conducted on a TA instruments model DSC Q2000 with a nitrogen (N_2) flow of 60 ml.min^{-1}. Analysis were performed on *Tzero* hermetic type pan (Figure 44). The samples were weighed directly in the pans and then sealed with a lid cover in the *Tzero* press (Figure 45).

Figure 44 - Tzero hermetic pan and lid.

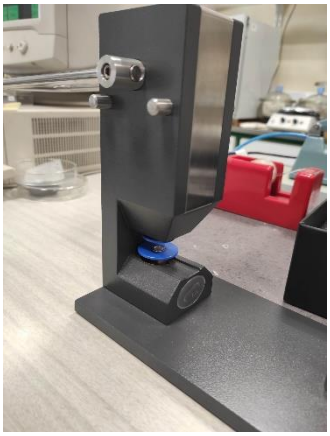

Figure 45 - Tzero press.

After this, the sample pan was placed inside the instrument together with the reference pan & lid (previously weighed), and the heating method was started. The thermal program used was:

1. Equilibrate at 30 ºC
2. Ramp 10 ºC.min^{-1}, to 150 ºC
3. Isothermal for 5 min
4. Ramp 10 ºC.min^{-1}, to -30 ºC
5. Ramp 10 ºC.min^{-1}, to 150 ºC

The first ramp at 10 ºC.min^{-1}, reference heating rate, to 150 ºC helps the polymer's structure reorganize, eliminating its thermal history and allowing an easier identification of the respective T_g. On the second ramp to 150 ºC, the T_g value is then registered. Thermal history is common in polymers like epoxy resin which have an exothermic polymerization and reach high temperatures.

4 Results and Discussion

4.1. Preliminary study

A preliminary study was conducted to assess the optimal doses of gamma radiation, both in the radiation-assisted cure and post-cure, to be used later in radiation after 2 and 10 days and for post-cure irradiation. This study was performed through thermogravimetric analysis of composite samples fully cured and still curing, irradiated with different doses of gamma radiation (0.5 kGy to 10 kGy).

The results from TGA are shown in Figures 46 and 47:

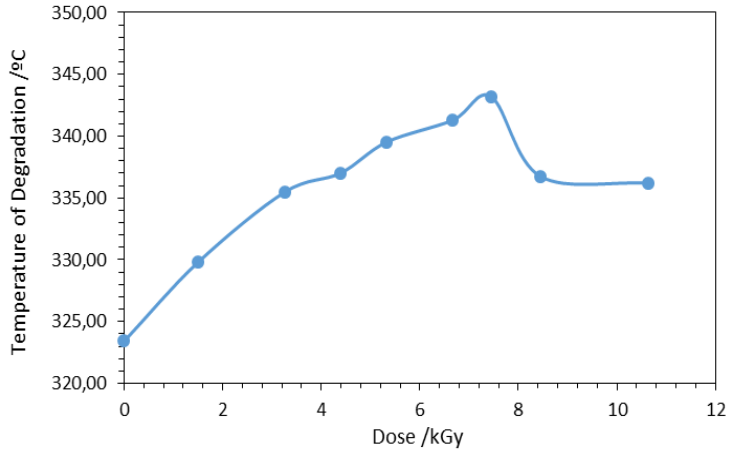

Figure 46 - Preliminary TGA results for post-cure irradiated composites at different doses of radiation.

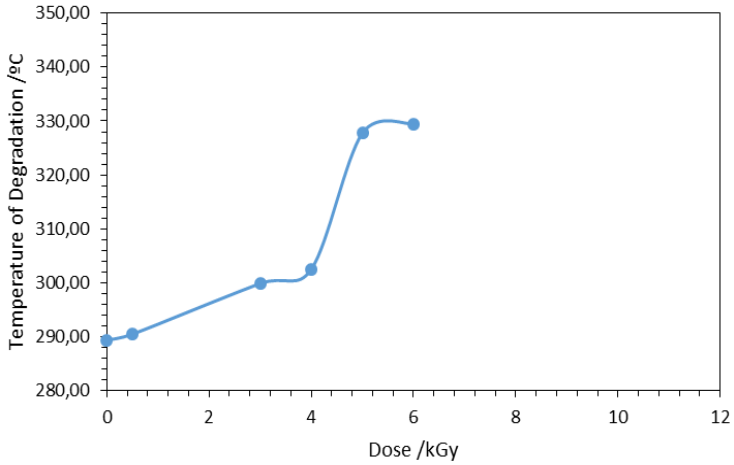

Figure 47 - Preliminary TGA results for composites irradiated during cure at different doses of radiation.

TGA curves show that the effect of gamma irradiation on the increment of the degradation temperature of the composite, for both situations, is more pronounced in the range between 4 and 7 kGy, with its maximum effect at 6-7 kGy. So, this dose range was selected to test the composite specimens under the 3 irradiation methodologies already stated.

4.2. Irradiation Results

As stated before, the tensile and bending specimens were divided for the three irradiation methodologies, *post-cure irradiation, irradiation after 2 days and irradiation after 10 days*. For each methodology, the specimens were subjected to gamma irradiation in the optimal dose range (4 to 7 kGy) selected in the preliminary study. D_{max} and D_{min} values were registered using PMMA routine dosimeters. Table 3 resumes these results.

Table 3 - Radiation results.

IRRADIATION METHODOLOGY	EXPECTED DOSE [kGy]	TENSILE TEST SPECIMENS				BENDING TEST SPECIMENS			
		Dmin [kGy]	Dmax [kGy]	Dm [kGy]	U	Dmin [kGy]	Dmax [kGy]	Dm [kGy]	U
POST-CURE	4	4.10	4.50	4.30	1.10	3.95	3.95	3.95	1.00
	5	5.08	5.61	5.35	1.10	4.94	5.00	4.97	1.01
	6	5.89	6.31	6.10	1.07	5.50	5.92	5.71	1.08
	7	7.13	7.78	7.46	1.09	6.96	7.06	7.01	1.01
2 DAYS	4	4.11	4.23	4.17	1.03	4.11	4.23	4.17	1.03
	5	5.08	5.55	5.32	1.09	5.08	5.55	5.32	1.09
	6	6.17	6.38	6.28	1.03	6.17	6.38	6.28	1.03
	7	7.33	7.91	7.62	1.08	7.33	7.91	7.62	1.08
10 DAYS	4	4.11	4.52	4.32	1.10	4.11	4.52	4.32	1.10
	5	5.00	5.64	5.32	1.13	5.00	5.64	5.32	1.13
	6	6.19	6.85	6.52	1.11	6.19	6.85	6.52	1.11
	7	7.13	7.50	7.32	1.05	7.13	7.50	7.32	1.05

The dose uniformity values presented in table 3 were all close to 1. This means that the dose distribution study and irradiation supports designed by (Soares, 2021) systematically provide uniform radiation distribution along the test specimens.

4.3. Mechanical Properties

4.3.1. Tensile Testing

This section will analyze changes in the composite mechanical properties through tensile testing resulting from irradiation in three different stages of the curing process (after 2 days, after 10 days, and post-cure). For this, properties like failure load, elongation at break and Young's modulus were considered to evaluate any significant changes in the material caused by gamma radiation.

4.3.2. Failure Load

Failure load is the load at which the material will fail catastrophically, causing a rupture.

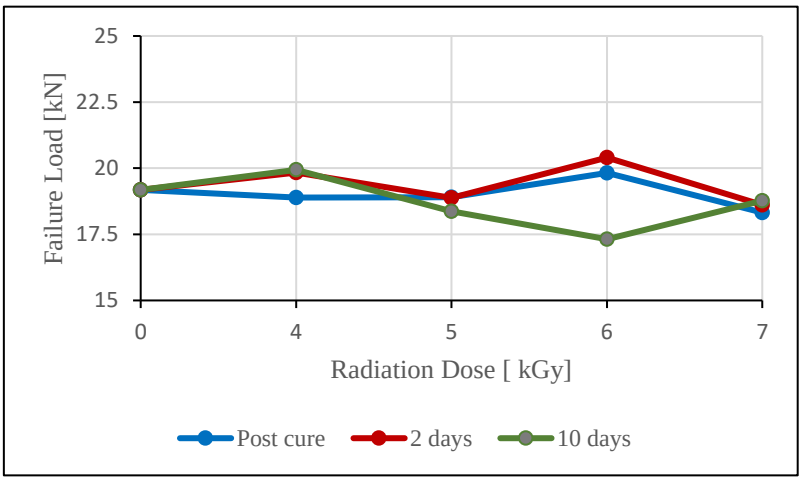

Figure 48 – Tensile failure load of the non-irradiated specimens and the specimens irradiated under three radiation methodologies at 4,5,6 and 7 kGy.

Figure 48 represents the variation of the failure load for each dose of radiation for the three irradiation processes to which the test specimens were subjected. When analyzing the graph, we can see that the failure load varies between 17.3 kN and 20.4 kN. The minimum load registered was 17.3 kN at 6 kGy after 10 days; the maximum load registered was 20.4 kN at 6 kGy after 2 days. These values correspond to a decrease of 9.74 % and an increase of 6.34 %, respectively, compared to the non-irradiated test specimens.

Post-cure irradiation shows a small improvement compared to the non-irradiated samples at 6 kGy (3.32 %); irradiation after 10 days has a similar improvement of 3.92 % at 4 kGy; irradiation after 2 days has the biggest improvement of the three (6.34 %).

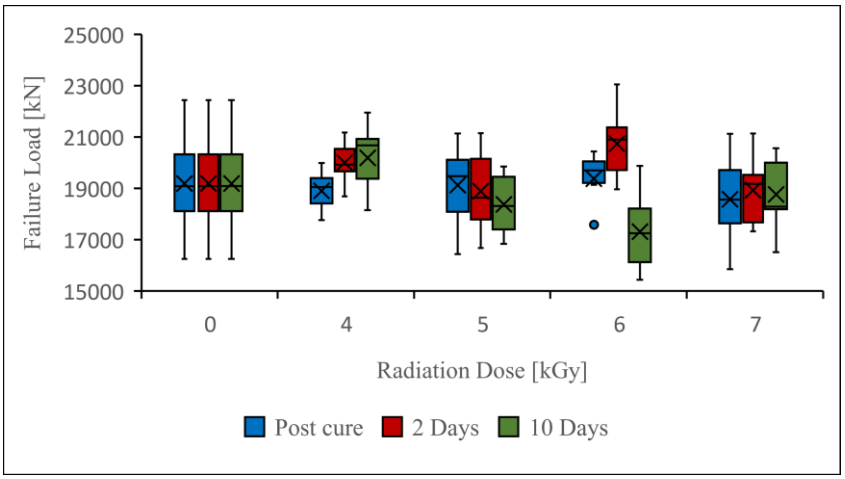

Figure 49 – Box and whisker plot of the tensile failure load for the non-irradiated specimens and the specimens irradiated under three radiation methodologies at 4,5,6 and 7 kGy.

In Figure 49, we can see a big dispersion of values between the three methods and doses. The standard deviation (STD) varies between 3.30 % for 4 kGy after 2 days and 8.61 % for 6 kGy after 10 days. The irradiation after 10 days has the worst overall uniformity between all doses of radiation (average 6.81 % STD). There is a better uniformity for the specimens irradiated after 2 days, even though the STD at 5 kGy is 7.9 %.

As a general rule, a constant increase in the failure load would be expected up to a certain dose and then start decreasing. However, the high STD evidences a lack of homogeneity in some test specimens. The lack of homogeneity might explain why the irradiation after 10 days decreases between 5 and 6 kGy and then goes up again at 7 kGy. The same happens at 5 kGy after 2 days.

Despite this, the failure load increases for at least one dose in each method, suggesting a prevalence of crosslinking over scissioning in some irradiated specimens, namely post-cure irradiation at 6 kGy, irradiation after 2 days at 4 and 6 kGy and irradiation after 10 days at 4 kGy.

4.3.3. Young's modulus

Young's modulus measures the ability of the material to withstand deformations when under a certain load.

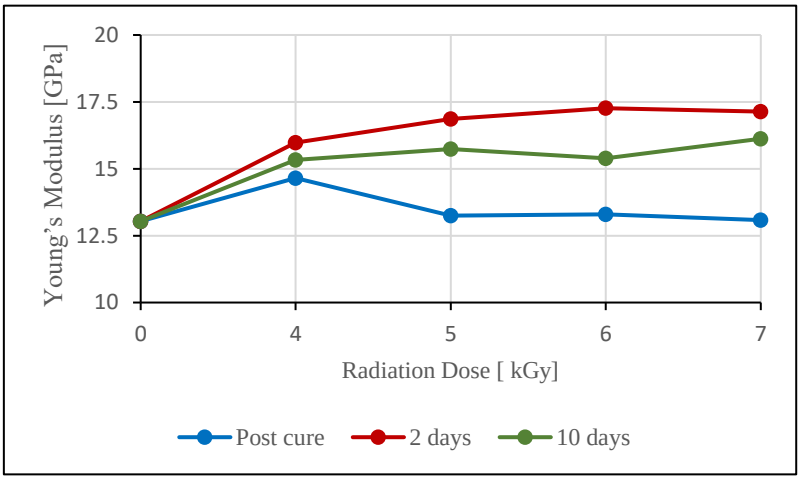

Figure 50 – Young's modulus of the non-irradiated specimens and the specimens irradiated under three radiation methodologies at 4,5,6 and 7 kGy.

Figure 50 represents the evolution of Young's modulus for each dose of radiation for the three irradiation processes to which the test specimens were subjected. When analyzing the graph, we can see that Young's modulus values vary between 13.04 GPa and 17.26 GPa. The minimum Young's modulus registered was 13.037 GPa on the non-irradiated specimens; the maximum Young's modulus registered was 17.263 GPa at 6 kGy after 2 days which corresponds

to an increase of 32.36 %. Post-cure irradiation has the smallest improvement compared to the non-irradiated samples at 4 kGy (12.38 %); irradiation after 10 days has an improvement of 23.66 % at 7 kGy; irradiation after 2 days has the biggest improvement of the three (32.36 %) at 6 kGy.

The increase in Young's modulus means that the material has become more resistant to permanent deformation. The material reaches a peak from post-cure irradiation at 4 kGy and then stabilizes in a downward trend. For irradiation after 2 days, there is steady growth from 4 to 6 kGy. For irradiation after 10 days, Young's modulus keeps increasing until 7 kGy with a slight drop at 6 kGy. It seems that the scissioning effect of gamma radiation becomes prevalent over crosslinking for higher doses than those stated. Despite this, there is an improvement in Young's modulus of all specimens.

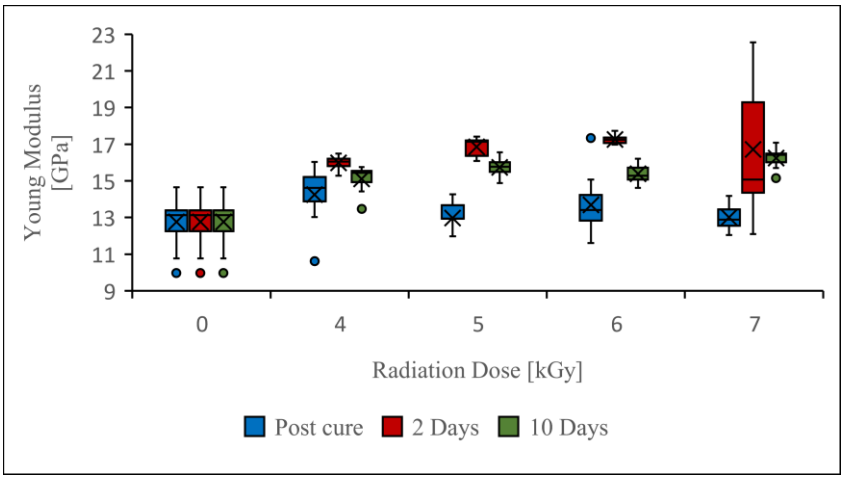

Figure 51 – Box and whisker plot of the Young's modulus for the non-irradiated specimens and the specimens irradiated under three radiation methodologies at 4,5,6 and 7 kGy.

In Figure 51, we can see that the standard deviation varies between 1.34 % for 6 kGy and 20.62 % for 7 kGy after 2 days. Irradiation after 2 days has the worst overall uniformity among all doses of radiation (average 6.77 % STD) as a consequence of the high dispersion of values at 7 kGy. Post-cure irradiation average STD is 6.03 %. On the other hand, the specimens irradiated after 10 days show a better STD of 3.26 %.

The evolution of Young's modulus (Figure 51) increases and then decreases as expected, unlike what happens in the failure load (Figure 49). The lower values of STD show a better uniformity of results.

4.3.4. Elongation at break

Elongation at break is the ratio between the initial length and the length after the breakage of the material. It is the capability to resist changes in shape without breaking.

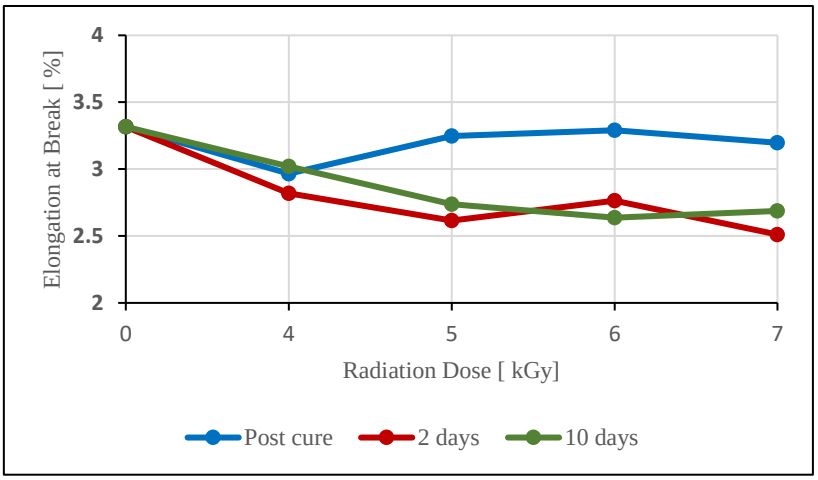

Figure 52 – Elongation at break of the non-irradiated specimens and the specimens irradiated under three radiation methodologies at 4,5,6 and 7 kGy.

Figure 52 represents the evolution of the elongation at break for each dose of radiation for the three irradiation processes to which the test specimens were subjected. When analyzing the graph, we see that the elongation values vary between 2.51 % and 3.32 %. The maximum elongation of 3.29 % was registered in the non-irradiated specimens; the minimum elongation of 2.51 % was registered at 7 kGy after 2 days which corresponds to a 24.27 % decrease compared to the non-irradiated test specimens. The decrease in the elongation at break was observed in three processes for all doses, which means the material has become stiffer after being exposed to gamma radiation and hence more resistant to stretch when a load is applied. These results are a clear sign of composites' crosslinking.

Elongation at break and Young's modulus are inversely proportional, which means that a decrease in elongation translates as an increase in Young's modulus. This can be stated in Figures 50 and 52.

The STD varies between 0,88 % for the non-irradiated specimens and 6,25 % for 6 kGy after 2 days. This high STD evidences a lack of homogeneity in some test specimens. This might be the reason for the rise at 6 kGy after 2 days instead of maintaining the downward tendency. Also, the irradiation after 2 days has the worst overall uniformity among all doses of radiation (average 4.98 % STD). The STD values at 5 and 6 kGy after 10 days are also high, 5.69 % and 6.13 %, respectively.

4.4. Flexural Testing

This section analyzed changes in the mechanical properties through flexural testing caused by irradiation in the three different stages of the curing process. For this, properties like failure load, flexural modulus and strain were considered to evaluate any significant changes in the material caused by gamma radiation.

4.4.1. Failure Load

Failure load is the load at which the material will fail catastrophically, causing a rupture.

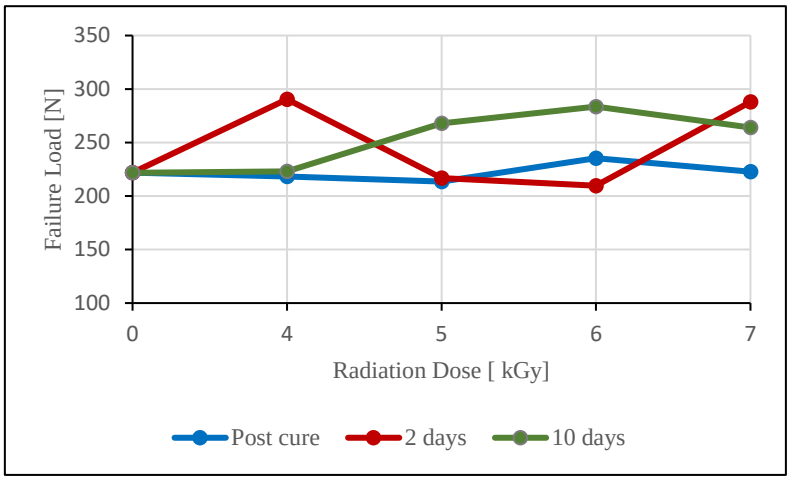

Figure 53 – Flexural failure load of the non-irradiated specimens and the specimens irradiated under three radiation methodologies at 4,5,6 and 7 kGy.

Figure 53 represents the variation of the failure load for each dose of radiation for the three irradiation processes to which the test specimens were subjected. When analyzing the graph, we can see that the failure load values vary between 209.7 N and 290.5 N. The minimum load of 209.69 N was registered at 6 kGy after 2 days; the maximum load of 290.47 N was registered at 4 kGy after 2 days. These values correspond to a decrease of 3.7 % and an increase of 30.98 %, respectively, compared to the non-irradiated test specimens.

Post-cure irradiation shows a small improvement compared to the non-irradiated samples at 6 kGy (6.14 %) but almost holds constant; irradiation after 10 days reaches a peak at 6 kGy with an improvement of 27.88 %; specimens irradiated after 2 days have the biggest improvement of the three (30.98 %).

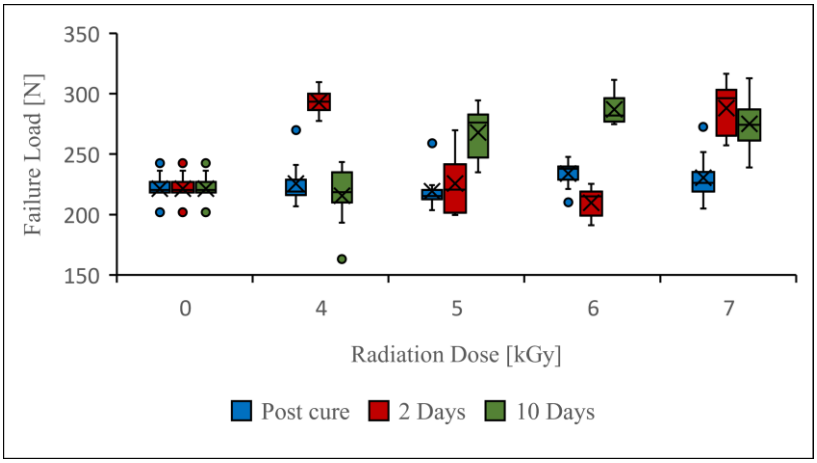

Figure 54 – Box and whisker plot of the flexural failure load for the non-irradiated specimens and the specimens irradiated under three radiation methodologies at 4,5,6 and 7 kGy.

In Figure 54, we can see a big dispersion of values between the three methods and doses. The standard deviation (STD) varies between 1.66 % for the non-irradiated specimens and 8.93 % for 7 kGy after 10 days. The irradiation after 10 days has the worst overall uniformity between all doses of radiation (average 7.04 % STD); irradiation after 2 days shows a similar average STD of 6.17 %. There is better uniformity for the post-cure specimens.

As a general rule, a constant increase in the failure load would be expected up to a certain dose and then start decreasing. However, the high STD evidences a lack of homogeneity in some test specimens. This might explain why the irradiation after 2 days decreases between 4 and 6 kGy and then goes up again at 7 kGy since the overall uniformity is low. Despite this, the failure load increases for at least one dose in each method, suggesting a prevalence of crosslinking over scissioning in some irradiated specimens, namely post-cure irradiation at 6 and 7 kGy, irradiation after 2 days at 4 and 7 kGy and irradiation after 10 days at all doses.

4.4.2. Flexural Modulus

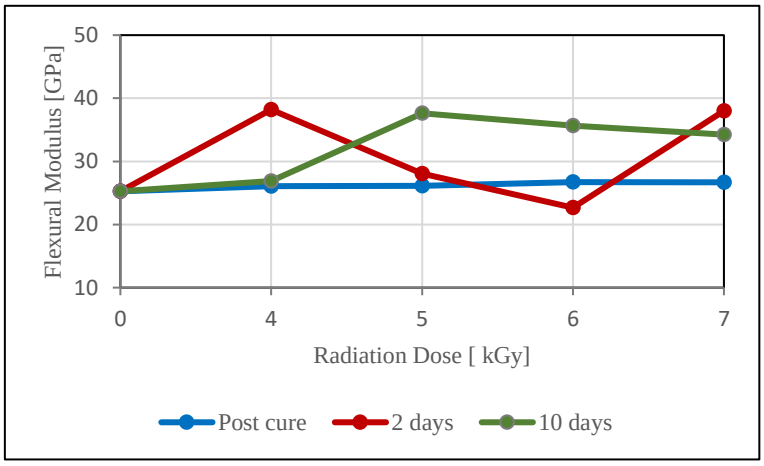

Figure 55 - Flexural modulus of the non-irradiated specimens and the specimens irradiated under three radiation methodologies at 4,5,6 and 7 kGy.

Figure 55 represents the evolution of flexural modulus for each radiation dose for the three irradiation processes the test specimens were subjected to. Analyzing the graph, we can see that the flexural modulus values vary between 22.67 and 38.2 GPa. The minimum and maximum modulus were registered at irradiation after 2 days; at 4 kGy, there is an increase of 51.23 %; at 6 kGy, there is a decrease of 10.26 %. Post-cure irradiation has the smallest improvement compared to the non-irradiated samples at 4 kGy (5.75 %); irradiation after 10 days reaches a peak at 5 kGy with an improvement of 48.9 %; irradiation after 2 days has the biggest improvement of the three, 51.23 %, at 4 kGy.

The increase in flexural modulus means that the material has become more resistant to flexion. Post-cure irradiation does not provide a big benefit with increasing doses of radiation because it maintains almost constant among all doses. For irradiation after 2 days, there is a peak at 4 kGy, which suddenly drops until 6 kGy, going up again at 7 kGy. For irradiation after 10 days, flexural modulus keeps increasing until 5 kGy and then stabilizes in a downward trend. This behavior suggests that scissioning effect of gamma radiation becomes prevalent over crosslinking for higher doses than those stated.

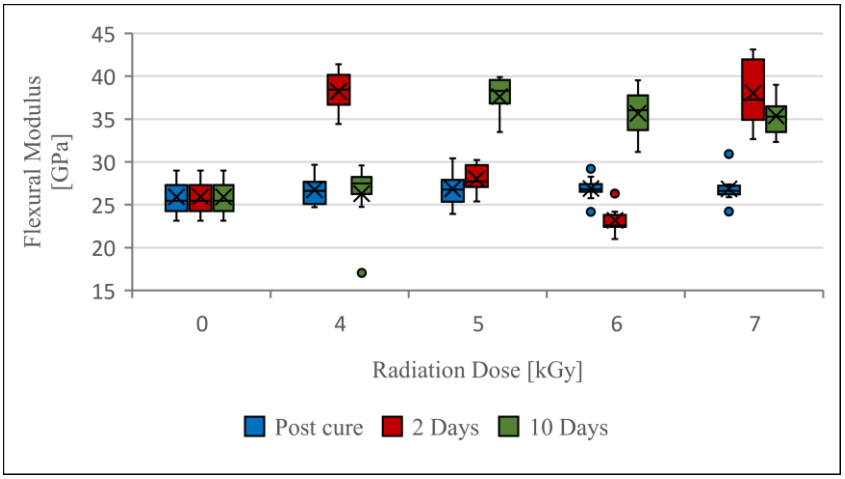

Figure 56 – Box and whisker plot of the flexural modulus for the non-irradiated specimens and the specimens irradiated under three radiation methodologies at 4,5,6 and 7 kGy.

In Figure 56, we can see that the standard deviation varies between 1.89 % and 10.03 %. Irradiation after 2 days has the worst overall uniformity among all doses of radiation (average 6.74 % STD) because there is a big dispersion of values at 4, 5 and 7 kGy. Irradiation after 10 days also shows a high value of STD (average 5.38 %). On the other hand, the post-cure specimens have a better STD of 3.29 %.

As a general rule, a constant increase in the modulus would be expected up to a certain dose and then start decreasing. However, the high STD evidences a lack of homogeneity in some test specimens. This might explain why the irradiation after 2 days decreases between 4

and 6 kGy and then goes up again at 7 kGy. Despite this, the modulus increases for almost all doses in each method, suggesting a prevalence of crosslinking over scissioning. The only modulus value lower than the non-irradiated specimens is 6 kGy after 2 days.

4.4.3. Flexural strain

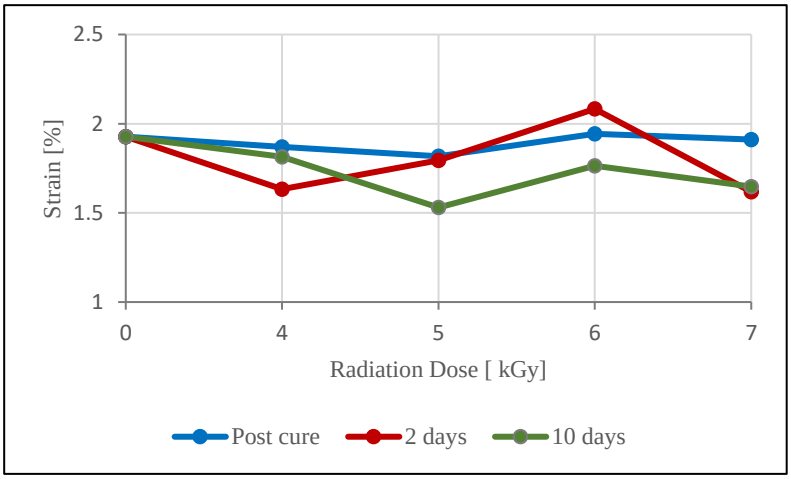

Figure 57 – Flexural strain of the non-irradiated specimens and the specimens irradiated under three radiation methodologies at 4,5,6 and 7 kGy.

Figure 57 represents the evolution of the strain for each dose of radiation for the three irradiation processes to which the test specimens were subjected. The graph shows that the strain values vary between 1.53 % and 2.08 %. The maximum elongation of 2.08 % was registered at 6 kGy after 2 days; the minimum elongation of 1.53 % was registered at 5 kGy after 10 days which corresponds to a 20.56 % decrease compared to the non-irradiated test specimens. The decrease in the elongation at break occurs for all doses after 10 days and for 4, 5 and 7 kGy after 2 days and post-cure. This means the material has become stiffer (for the stated doses) after being exposed to gamma radiation and hence more resistant to stretch when a load is applied. These results clearly show that the specimens suffer an added crosslinking by gamma irradiation.

Strain and flexural modulus are inversely proportional, which means that a decrease in strain translates as an increase in flexural modulus. This can be observed in Figures 55 and 57.

The STD varies between 0,88 % for the non-irradiated specimens and 6,25 % for 6 kGy after 2 days. The high STD evidences a lack of homogeneity in some test specimens. This might explain why there is a rise at 6 kGy instead of maintaining the downward tendency. Also, the irradiation after 2 days has the worst overall uniformity among all doses of radiation (average 4.98 % STD). The STD values at 5 and 6 kGy after 10 days are also high, 5.69 % and 6.13 %, respectively, evidencing a lack of homogeneity. This might be why the elongation at these doses is inferior to 7 kGy.

4.5. Thermal Properties

4.5.1. Thermogravimetric Analysis

According to work already performed (Soares, 2021), at temperatures between 700 and 900 ºC, only the epoxy resin part is degraded in the composite. Since the epoxy is the part of the composite that may suffer changes with radiation, there is no need to go to higher temperatures above that interval. Therefore, after a few preliminary assays conducted up to 1100 ºC for validation, all TGAs were recorded from room temperature (21 ºC with stabilization at 30 ºC) up to 800 ºC.

For each radiation dose and irradiation methodology, at least 2 thermograms were made from samples collected from the total number of specimens irradiated. Since it is not feasible to present all the TGA thermograms, the ones below are illustrative of the general behavior of each group of samples. As already stated, the samples necessary for each TGA run were collected from at least 5 different test specimens used in mechanical testing. The material collected from each specimen was then mixed to constitute a unique sample.

The method used to determine the degradation temperature, T_{deg}, was the "on-set point" according to ISO 11358/2014 – Thermogravimetry (T_g) of Polymers.

Figure 58 represents the thermal behavior of the non-irradiated composite. Figure 59 represents the thermal behavior of the composite irradiated after 2 days at a dose of 6 kGy, which has the maximum degradation temperature value registered.

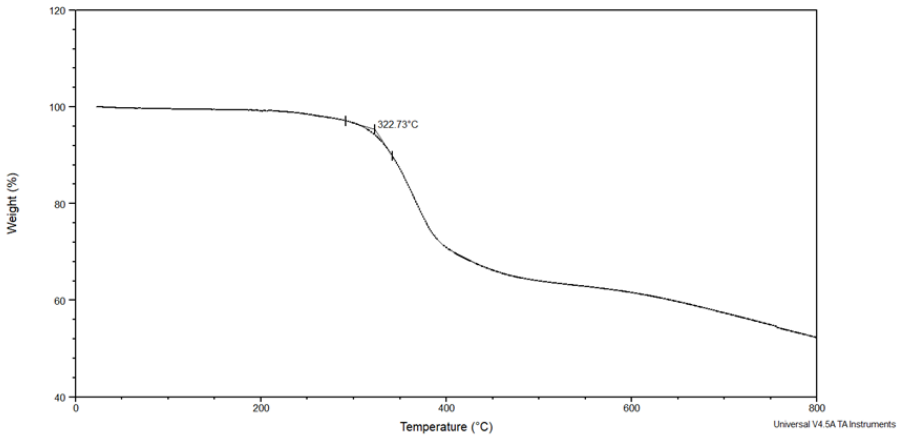

Figure 58 - Thermal behavior of the non-irradiated composite.

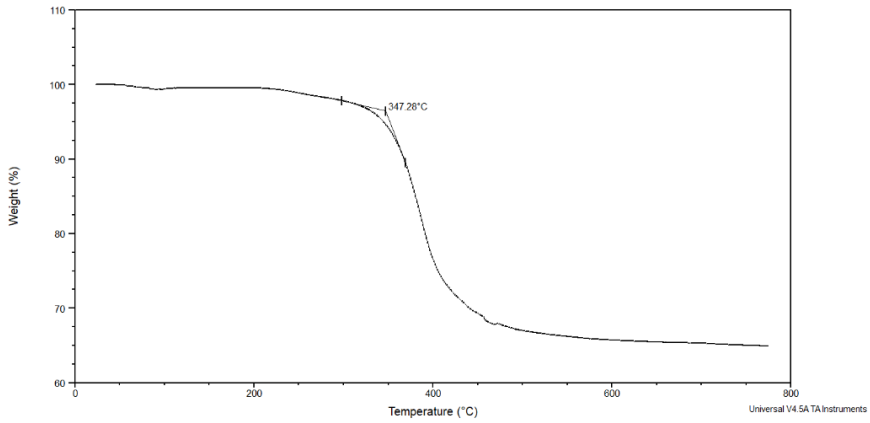

Figure 59 - Thermal behavior of the composite irradiated after 2 days at a dose of 6 kGy.

Figures 60 to 62 represent the general thermal behavior of the composite irradiated at different doses of gamma radiation according to the three irradiation methodologies. The thermal behavior of the non-irradiated composite is also displayed in each figure to serve as the control. The curves were overlaid to facilitate the comparison between each dose. It also helps identify the evolution of the degradation temperatures with the increase in radiation dose.

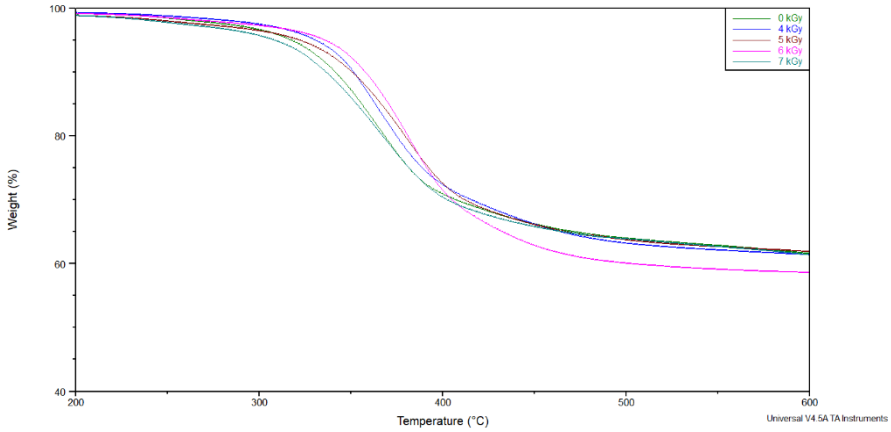

Figure 60 - Thermal behavior of the non-irradiated composite and the post-cure irradiated composite at 4,5,6 and 7 kGy

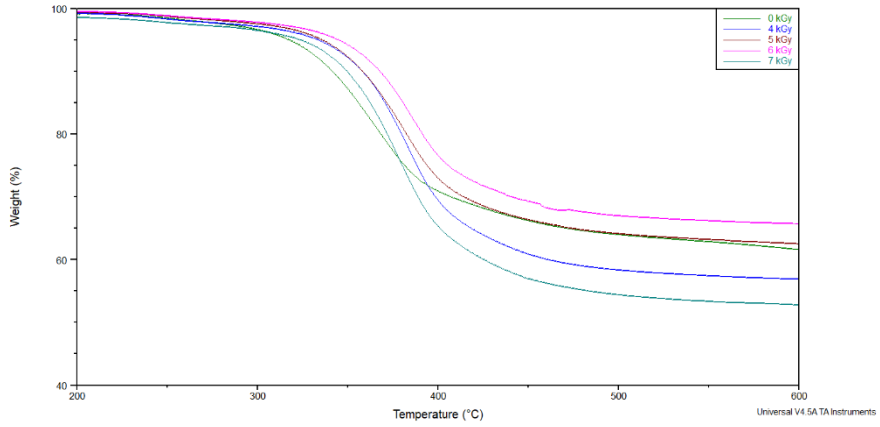

Figure 61 - Thermal behavior of the non-irradiated composite and the composite irradiated after 2 days at 4,5,6 and 7 kGy.

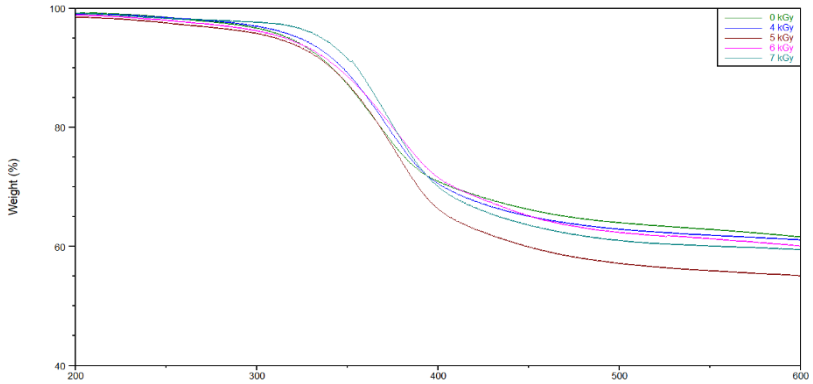

Figure 62 - Thermal behavior of the non-irradiated composite and the composite irradiated after 10 days at 4,5,6 and 7 kGy.

It is clear that with increasing doses of radiation, the lines tend to move to the right along the x-axis. This means that the composite's degradation temperature increases with radiation dose. For post-cure irradiation and irradiation after 2 days, the rightmost line is the one relative to 6 kGy. For irradiation after 10 days is the one relative to 7 kGy. This indicates that the composite irradiated at 6 kGy presents a higher degradation temperature. However, for irradiation after 10 days, the degradation temperature maintains an upward tendency until 7 kGy. These statements can also be verified in Figure 63:

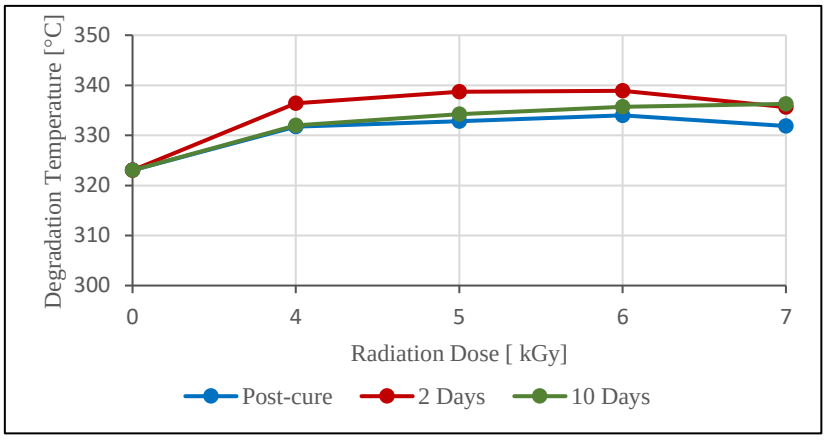

Figure 63 - Evolution of the degradation temperature with increasing doses of radiation for three irradiation methodologies.

Figure 63 represents the evolution of the degradation temperature of the composite for each radiation dose for the three irradiation methodologies the test specimens were subjected. The maximum degradation temperature registered was 338.9 °C at 6 kGy with irradiation after 2 days. This value translates as an increase of 16.5 °C (5.10 %). It can also be verified that for the same doses of radiation, irradiation after 2 days samples has higher values of $T_{deg,}$ followed by irradiation after 10 days and lastly by post-cure irradiation. Table 4 sums up the composite degradation temperatures for the three irradiation methodologies at 4, 5, 6 and 7 kGy and the non-irradiated specimens:

Table 4 – Degradation temperatures at different doses for 3 irradiation methodologies.

Irradiation Method	*Dose [kGy]*		*Tdeg [°C]*
	Expected Dose	Real Dose	
	0	0	322.43
Post-cure	4	4.3	331.49
	5	5.35	332.795
	6	6.1	333.995
	7	7.46	331.835
2 days	4	4.17	336.41
	5	5.32	338.675
	6	6.28	338.895
	7	7.62	335.615
10 days	4	4.32	331.965
	5	5.32	334.205
	6	6.52	335.675
	7	7.32	336.285

4.5.2. Differential Scanning Calorimetry

The glass transition temperatures of the epoxy part of the composite irradiated through the different methodologies were determined through DSC, and the thermograms obtained are presented below. Not being feasible to present all the DSC thermograms, the ones presented below are representative of the general behavior of each sample. The samples necessary for each DSC were collected the same way as the samples for the TGA assays.

The heating method described in chapter 3.5.2 is represented in Figure 64. The blue line corresponds to the first heating ramp from room temperature to 150 °C; then the red line represents the isothermal step for 5 minutes; in green, the second ramp from 150 ºC to -30 ºC and finally, in pink, the last heating ramp up to 150 ºC.

The area of the blue line peak corresponds to the amount of energy associated with the structural reorganization of the epoxy matrix, commonly associated with the elimination of the thermal history of the materials. On the last heating ramp (-30 ºC to 150 ºC), it is possible to register a more accurate and real value of the material's glass transition temperature.

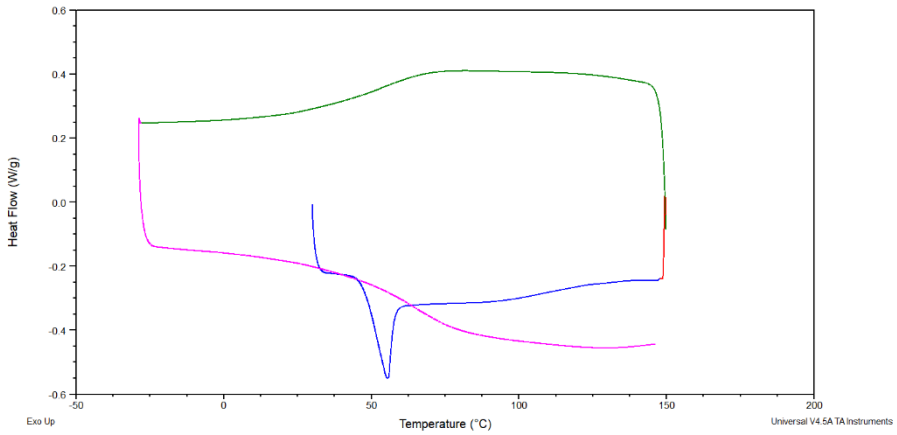

Figure 64 - DSC heating method of the non-irradiated specimens.

Figures 65, 66 and 67 represent the thermal behavior of the epoxy resin, the non-irradiated composite and the composite irradiated after 2 days at 5 kGy, respectively. Figure 67 was selected because it represents the maximum glass transition temperature value registered.

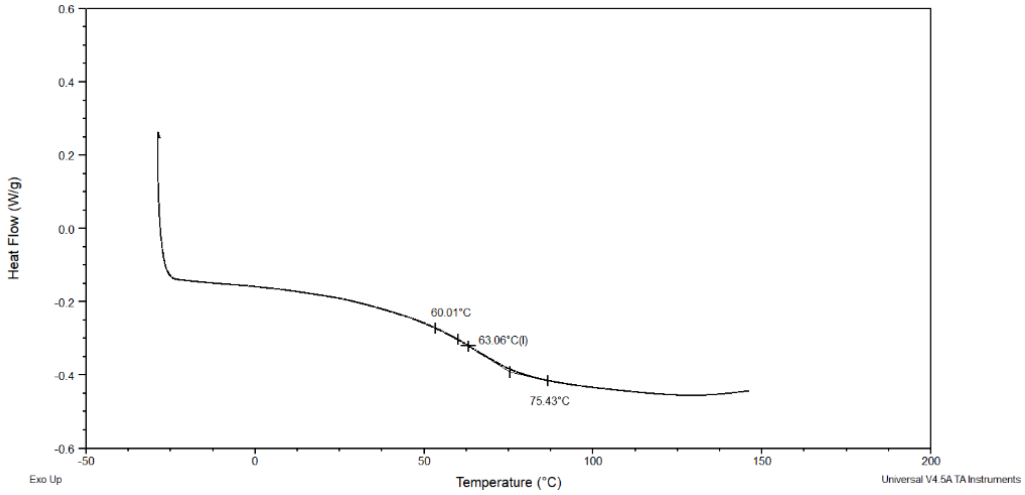

Figure 65 - Glass transition temperature of the non-irradiated epoxy resin.

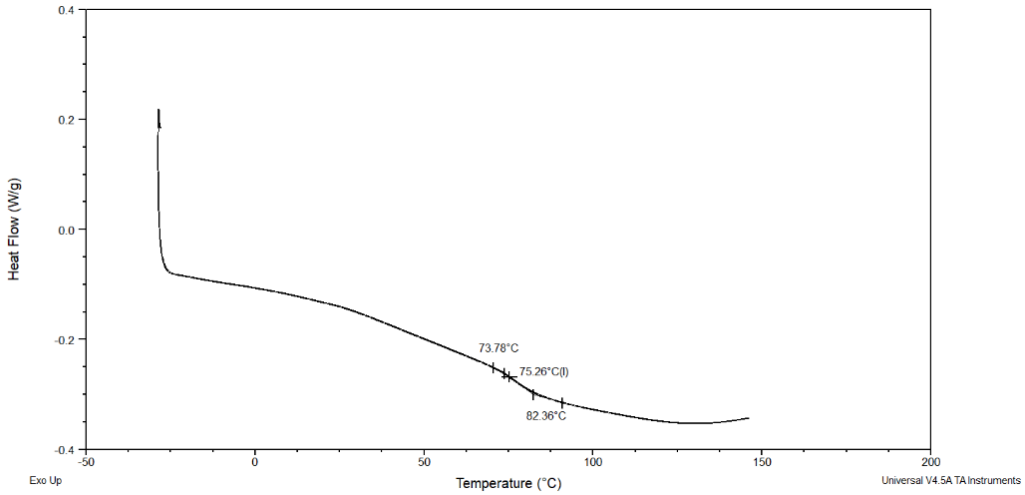

Figure 66 - Glass transition temperature of the non-irradiated composite.

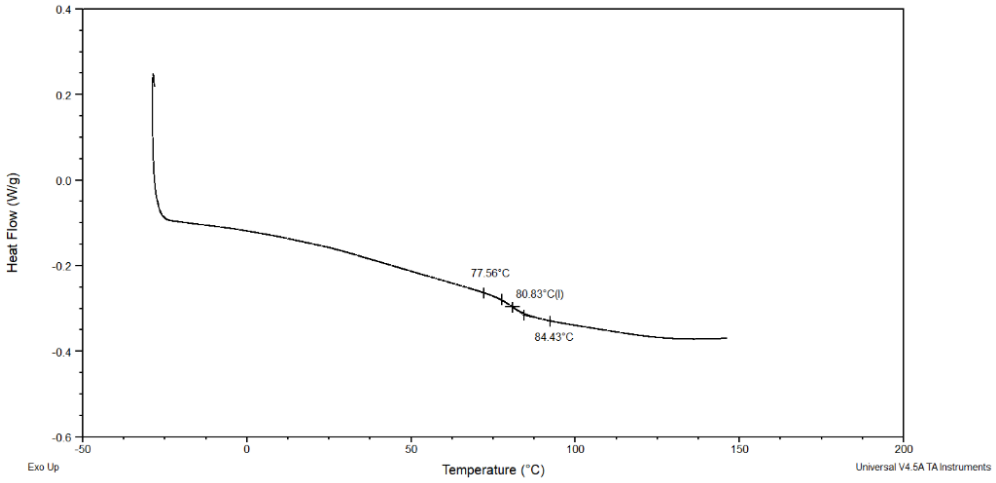

Figure 67 - Glass transition temperature of the composite irradiated after 2 days at 5 kGy.

Figures 68 to 70 represent the general thermal behavior of composite obtained from the three irradiation methodologies irradiated at different doses of gamma radiation, in the range of temperature between 30ºC and 150 ºC. The thermal behavior of the non-irradiated composite is also displayed in each figure to serve as the control. The curves were overlaid to facilitate the comparison between each dose. It also helps identify the evolution of the glass transition temperatures with the increase in radiation dose for each irradiation method.

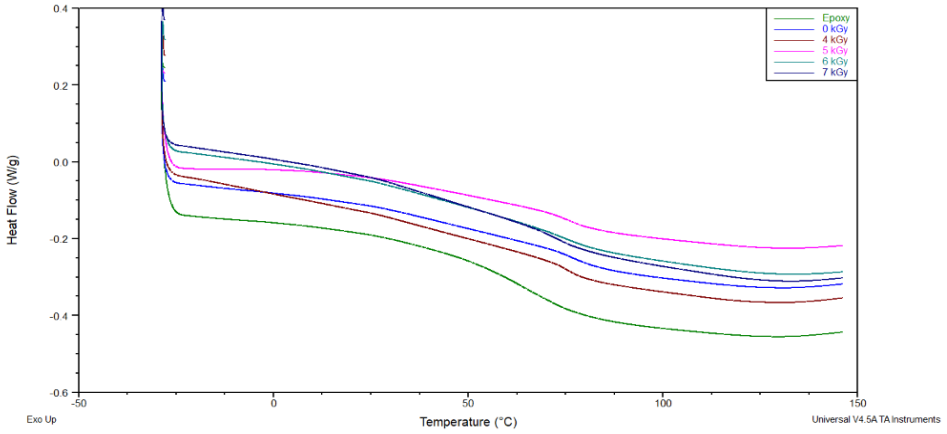

Figure 68 – DSC thermogram of the non-irradiated composite and the post-cure irradiated composite at 4,5,6 and 7 kGy.

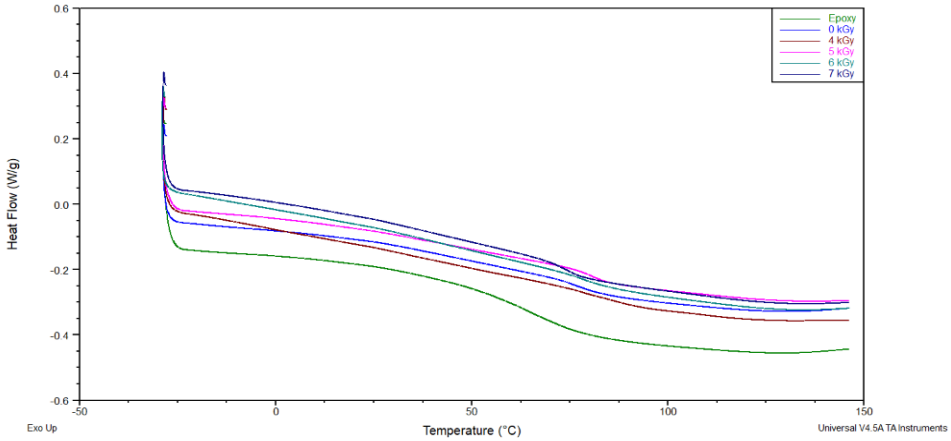

Figure 69 – DSC thermogram of the non-irradiated composite and the composite irradiated after 2 days at 4, 5, 6 and 7 kGy.

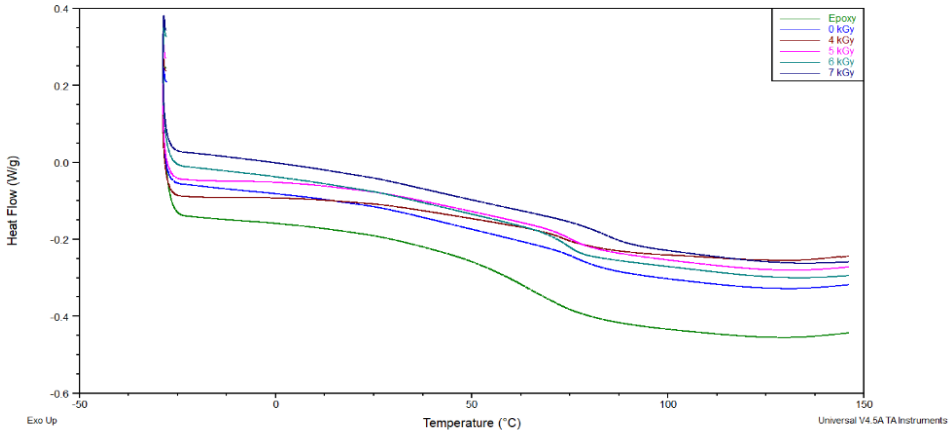

Figure 70 - DSC thermogram of the non-irradiated composite and the composite irradiated after 10 days at 4, 5, 6 and 7 kGy.

It is clear that with increasing doses of radiation, the lines tend to move to the right along the x-axis, which corresponds to an increment in the T_g of the composite epoxy matrix. For post-cure irradiation and irradiation after 2 days, the rightmost line is the one relative to 5 kGy. For irradiation after 10 days is the one relative to 7 kGy. This means that the glass transition temperature reaches a peak at 5 kGy and then assumes a downward tendency. However, for irradiation after 10 days, the glass transition temperature maintains almost constant until 6 kGy and then increases at 7 kGy. These statements can also be verified in Figure 71:

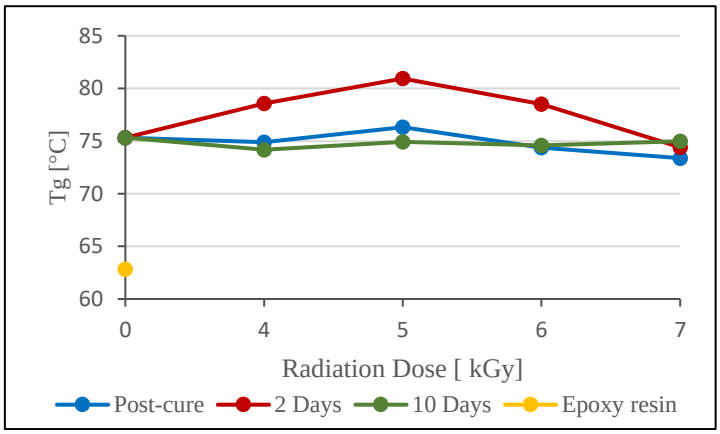

Figure 71 - Evolution of the degradation temperature with increasing doses of radiation for three irradiation methodologies.

The yellow dot in Figure 71 represents the T_g of the epoxy resin used to fabricate the laminates. The value obtained is 13 °C higher than the value announced by the manufacturer. However, the T_g values for the non-irradiated composite and the composite irradiated in three methodologies were lower than 90 °C (value announced by the manufacturer for a non-irradiated composite).

Figure 71 represents the evolution of glass transition temperature for each radiation dose for the three irradiation methodologies the test specimens were subjected. The maximum registered glass transition temperature was 80.94°C at 5 kGy after 2 days of irradiation. This value translates as an increase of 5.61°C (7.44 %). It can also be verified that for the same doses of radiation, irradiation after 2 days has higher values of T_g.

Table 5 sums up the values obtained from the thermal analysis for the three methodologies.

Table 5 – Thermal analysis results obtained through TGA and DSC of the epoxy resin, non-irradiated composite and irradiated composite under 3 irradiation methodologies at different radiation doses

Irradiation Methodology	**Material**	**Dose [kGy]**		**T_g [°C]**	**T_{deg} [°C]**
		Expected Dose	Real Dose		
	Epoxy Resin	-	-	62.81	-
	Composite	0	0	75.29	322.43
Post-Cure	Composite	4	4.30	74.88	331.49
		5	5.35	76.32	332.79
		6	6.10	72.51	333.99
		7	7.46	73.38	331.84
2 Days	Composite	4	4.17	78.56	336.41
		5	5.32	80.94	338.68
		6	6.28	78.51	338.89
		7	7.62	74.41	335.62
10 Days	Composite	4	4.32	74.18	331.97
		5	5.32	74.93	334.21
		6	6.52	74.60	335.68
		7	7.32	75.07	336.29

5 Conclusions and Future Work

5.1. Overview

Currently, with the technological progress in the aerospace industry, there is the need to find lighter and stronger materials that can overcome the difficulties posed by modern complex aircraft designs and fuel consumption. Composite materials that combine stiff fibers and high-performance resins are becoming the solution to this problem and are already replacing metals in aircraft's primary structures. The aviation industry is the most interested in these type of materials because, even with high prices, the weight saving is more important.

The tendency to replace metals with composite materials is stated in the civil aircraft industry, military aircraft, and UAVs. Modern aircraft already have more than 40 % of the total weight made of composites. They reduce weight and increase the mechanical properties, but they also reduce the detectability by radars, which is one of the requirements of 5^{th} generation fighter aircraft. UAVs acquired by the Portuguese military branches are mostly made of composites. In particular, the ones designed and fabricated at CIAFA are primarily made of carbon-epoxy composites through wet-layup. So, it is crucial to find new ways of improving their properties.

Radiation-induced crosslinking is already used in many applications, such as improving polymers' mechanical, thermic and chemical properties. In particular, radiation-assisted cure can significantly improve the properties of polymers through crosslinking.

The focus of this dissertation was to compare the effects of radiation-assisted cure (in 2 different phases of the curing process) to post-cure irradiation on the functional properties of carbon-epoxy composites. To compare these effects, the test specimens were analyzed through tensile and flexural testing, thermogravimetric analysis and differential scanning calorimetry to obtain properties such as flexural and Young's modulus, failure loads, degradation temperature and glass transition temperature.

The test specimens were fabricated from laminates made with a 3K carbon mat with 160 $g.m^{-2}$ and a two-component resin SR8200 with SD7206 hardener through wet-layup. In each laminate, the first layer is set on the glass panel and impregnated with the resin. Subsequently, new layers are then applied and impregnated over each other using a paint roller. The laminate stayed in the vacuum bag curing for at least 24 hours before being cut in the CNC machine. The test specimens for tensile and flexural testing were then cut in the CNC machine according to ISO 527-4/2020 and ISO14125/2011, respectively. The samples for TGA and DSC were also collected from these test specimens after the tensile and flexural testing.

5.2. Conclusions

A preliminary study was done to assess the optimal doses of gamma radiation, both in the radiation-assisted cure and post-cure, to be used later in radiation after 2 and 10 days and for post-cure irradiation. This study was performed through thermogravimetric analysis of composite samples fully cured and still curing, irradiated with different doses of gamma radiation (1.5 kGy to 10 kGy). This study showed that the range between 4 and 7 kGy provided the highest degradation temperatures to the material. So, it was selected to irradiate the test specimens under the three irradiation methodologies.

The mechanical and thermal tests show improvements in the carbon-epoxy composite properties that were irradiated through controlled exposition to gamma radiation compared to the non-irradiated composites. There are also improvements between the three irradiation methodologies.

The tensile testing values suggest that irradiation after 2 days provides higher values of failure load and Young's modulus and lower elongation at break compared to irradiation after 10 days and post-cure irradiation. Post-cure irradiation is the methodology that is least beneficial of the three. Irradiation after 2 days provides an increase of 6.34 % in the failure load, a 32.36 % increase in Young's modulus and a decrease of 24.27 % in elongation at break. Concerning the radiation doses, 6 kGy seems to be the limit at which crosslinking still overlaps chain scission. Higher doses start reducing the overall properties of the composite. Failure load values did not follow the expected increase up to a certain dose at which its values would start decreasing; the values where this happens show a high STD of 7 to 8 %.

There is no evidence of the optimal radiation dose concerning flexural testing since it is different for each irradiation methodology. However, the dose that registered better values was 4 kGy with irradiation after 2 days. This seems to be the most beneficial irradiation methodology, similar to tensile testing, followed by irradiation after 10 days and lastly, post-cure irradiation. Irradiation after 2 days provides an increase of 30.98 % in the failure load and a 51.23 % increase in flexural modulus. The highest decrease of flexural strain was 20.56 % for irradiation after 10 days. The values obtained for the three flexural properties analyzed do not follow the expected trend with increasing radiation doses, which, once again, might be related to the lack of homogeneity in the test specimens. The values where this happens show a high STD of 6 to 10 %.

According to the TGA results, the irradiation after 2 days provides higher values of T_{deg} for most radiation doses, followed by irradiation after 10 days and post-cure, respectively. The maximum T_{deg} registered was 338.9 °C at 6 kGy, translating into an increase of 16.5 °C

(+5.10%) compared to non-irradiated specimens. The optimal dose seems to be 6 kGy; the thermal behavior profiles obtained evidence that at higher radiation doses, chain-scission starts overlapping crosslinking with the consequent decrease of thermal resistance. For irradiation after 10 days, the T_{deg} continues increasing until 7 kGy.

DSC technique shows that the T_g increases to 80.94 °C (7.44 %) at 5 kGy with irradiation after 2 days. Again, this irradiation methodology provides higher values than the other methodologies. The optimal radiation dose seems to be 5 kGy. Post-cure irradiation and irradiation after 10 days did not show significant increases in the $T_{g.}$

Comparing the mechanical and thermal analysis, it was clear that radiation-assisted cure was more effective at providing better properties to the treated material than post-cure irradiation. Particularly, irradiation after 2 days provided better properties among the three methodologies tested. Also, 5 and 6 kGy were the radiation doses that provided the higher properties values among the three methodologies tested.

The lack of structural homogeneity in the tested specimens seemed to be one of the limitations of this study. Bad dispersion of resin in the composite and some superficial flaws were clear to the naked eye. This might be related to a not efficient adhesion between the resin and the carbon fiber. In addition, the SR8200 resin and SD7206 hardener are new at CIAFA since the normally used resin was discontinued. Therefore, the fact that this resin is new was also a limitation of this study. Furthermore, this resin did not show compatibility with carbon as well as the previously used resin.

5.3. Future work

Radiation-assisted cure provided better results than post-cure irradiation, which until now was the only study made by the Portuguese Air Force related to the improvement of carbon-epoxy composites using gamma radiation. Radiation-assisted cure should be studied in depth to extend the work developed in this dissertation. This study analyzed radiation-assisted cure in the initial phase of curing and on the last day of curing (according to the cure schedule provided by the manufacturer). Analyzing this methodology in an intermediate phase might be more efficient.

The laminate fabrication process should be revised in order to produce a more homogenous material with fewer superficial flaws. Adding the reinforcement tabs posterior to the initial 24 hours cure might help maintain the vacuum pressure equal along the laminate, improving the overall homogeneity.

This study also showed that the adhesion between this resin and carbon fiber is not as good as the previously used resin at CIAFA. Adding an interface between the fiber and resin, such as graphene, might improve their adhesion. In addition, the influence of radiation-assisted cure in the resin, with the addition of an interface, should be tested to assess any possible improvements. Research has developed techniques that used graphene only as a mixing constituent in the composite material to complex examples where graphene is covalently bonded to the carbon fiber, matrix or both (Keyte et al., 2019). Graphene or carbon nanotubes can modify the carbon fiber-reinforced epoxy composites to improve and enhance the electrical and thermal conductivities (Alemour et al., 2019).

Bibliography

Alemour, B., Badran, O., & Hassan, M. R. (2019). A Review of Using Conductive Composite Materials in Solving Lightening Strike and Ice Accumulation Problems in Aviation. *Journal of Aerospace Technology and Management*, *11*, 1–23. https://doi.org/10.5028/jatm.v11.1022

ASM International. (2004). *Introduction to Tensile Testing* (J. R. Davis (Ed.)). ASM International.

ASTM International. (2002). Standard Test Methods for Flexural Properties of Unreinforced and Reinforced Plastics and Electrical Insulating Materials. *Annual Book of ASTM Standards*, *April*, 1–11. https://doi.org/10.1520/D0790-10.

Bielawski, R. (2017). Composite Materials in Military Aviation and Selected Problems With Implementation. *Review of the Air Force Academy*, *15*(1), 11–16. https://doi.org/10.19062/1842-9238.2017.15.1.2

Boeing: 787 Dreamliner. (n.d.). Retrieved May 29, 2022, from https://www.boeing.com/commercial/787/

Bolton, W., & Higgins, R. A. (2014). Materials for Engineers and Technicians. In *Materials for Engineers and Technicians*. https://doi.org/10.4324/9781315771687

Callister, W. D., & Rethwisch, D. G. (2017). Materials Science and Eng. *Materials Science and Engineering: A*, 251–270.

Chung, D. D. L. (2010). *Composite Materials: Science and Applications* (B. Derby (Ed.); Second). Springer. https://doi.org/10.1007/978-1-84882-831-5

Cleland, M. R., Parks, L. A., & Cheng, S. (2003). Applications for radiation processing of materials. *Nuclear Instruments and Methods in Physics Research, Section B: Beam Interactions with Materials and Atoms*, *208*(1–4), 66–73. https://doi.org/10.1016/S0168-583X(03)00655-4

Cowie, J. M. G., & Arrighi, V. (2007). *Polymers: Chemistry and Physics of Modern Materials* (Third). CRC Press.

Deokar, S., & Visal, S. (2019). *A Review Paper on Properties of Carbon Fiber Reinforced Polymers*. *May 2016*. www.ijirst.org

Drobny, J. G. (2003). *Radiation Technology for Polymers*. CRC Press.

Drobny, J. G. (2012). Ionizing Radiation and Polymers: Principles, Technology, and Applications. In *Ionizing Radiation and Polymers: Principles, Technology, and Applications*. https://doi.org/10.1016/C2011-0-05010-X

Ferreira, L. M. M. (2008). *Modificação de polietileno por copolimerização de enxerto induzida por radiação gama : sua aplicação na área dos biomateriais* [Lisbon University]. https://doi.org/10.29327/523696.1-1

Gay, D., Hoa, S. V., & Tsai, S. W. (2003). Composite materials: Design and applications. In *Composite Materials: Design and Applications*. CRC Press.

General Dynamics to build wide-band radomes for F-16s | Shephard. (n.d.). Retrieved May 25, 2022, from https://www.shephardmedia.com/news/digital-battlespace/general-dynamics-build-wide-band-radomes-f-16s/

Groeneveld, T., & Elsea, A. (2009). Mechanical Testing Methods. *Hydrogen Embrittlement Testing*, 11-11–19. https://doi.org/10.1520/stp38925s

Hang, X., Li, Y., Xiaozhong, H., li, N., & Wen, Y. (2015). Effects of temperature profiles of microwave curing processes on mechanical properties of carbon fibre–reinforced composites. *Proceedings of the Institution of Mechanical Engineers, Part B: Journal of Engineering Manufacture*, *231*. https://doi.org/10.1177/0954405415596142

Hsissou, R., Seghiri, R., Benzekri, Z., Hilali, M., Rafik, M., & Elharfi, A. (2021). Polymer composite materials: A comprehensive review. *Composite Structures*, *262*(November 2020). https://doi.org/10.1016/j.compstruct.2021.113640

International Organization for Standardization. (1999). *ISO 11357-2 - Plastics - Differential scanning calorimetry (DSC) - Part 2: Determination of glass transition temperature*. https://www.iso.org/standard/25545.html

International Organization for Standardization. (2011). *ISO 14125 - Fibre-Reinforced plastic composites - Determination of flexural properties*. https://www.iso.org/standard/52874.html

International Organization for Standardization. (2019). *ISO 527-1 - Plastics - Determination of tensile properties - Part 1: General principles*. https://www.iso.org/standard/75824.html

International Organization for Standardization. (2020). *ISO/DIS 527-4 - Plastics - Determination of tensile properties - Part 4: Test conditions for isotropic and orthotropic fibre-reinforced plastic composites*. https://www.iso.org/standard/80369.html

International Organization for Standardization. (2022). *ISO 11358-1 - Plastics - Thermogravimetry (TG) of polymers - Part 1: General principles.* https://www.iso.org/standard/79999.html

Keyte, J., Pancholi, K., & Njuguna, J. (2019). Recent Developments in Graphene Oxide/Epoxy Carbon Fiber-Reinforced Composites. *Frontiers in Materials*, *6*(October), 1–30. https://doi.org/10.3389/fmats.2019.00224

Khoe, C., Sen, R., & Bhethanabotla, V. (2011). Oxygen Permeability of Fiber-Reinforced Polymers. *Journal of Composites for Construction*, *15*, 513–521. https://doi.org/10.1061/(ASCE)CC.1943-5614.0000187

Latteier, P. (2019). *Carbon Fiber Weaves: What they are and why to use them - Elevated Materials*. https://www.elevatedmaterials.com/carbon-fiber-weaves-what-they-are-and-why-to-use-them/

Makuuchi, K., & Cheng, S. (2011). Radiation Processing of Polymer Materials and its Industrial Applications. In *Radiation Processing of Polymer Materials and its Industrial Applications*. https://doi.org/10.1002/9781118162798

Mallick, P. K. (2007). Fiber-reinforced composites - Materials, Manufacturing and Design. In *Concrete Construction Engineering Handbook, Second Edition* (Third). CRC Press.

Mangalgiri, P. D. (1999). Composite materials for aerospace applications. *Bulletin of Materials Science*, *22*(3), 657–664. https://doi.org/10.1007/BF02749982

Menczel, J. D., & Bruce Prime, R. (Eds.). (2008). *Thermal Analysis of Polymers - Fundamentals and Applications*. Wiley. https://doi.org/10.1002/9780470423837

Menczel, J. D., Judovits, L., Prime, R. B., Bair, H. E., Reading, M., & Swier, S. (2009). Differential Scanning Calorimetry (DSC). In *Thermal Analysis of Polymers* (pp. 7–239). John Wiley & Sons, Ltd. https://doi.org/https://doi.org/10.1002/9780470423837.ch2

Menczel, J. D., Prime, R. B., & Gallagher, P. K. (2009). Introduction. In *Thermal Analysis of Polymers* (pp. 1–6). John Wiley & Sons, Ltd. https://doi.org/https://doi.org/10.1002/9780470423837.ch1

Rami, N., Meghraoui, H., Ziraoui, R., El khoukhi, T., Mouhib, M., & El Harfi, A. (2010). Influence of gamma irradiation on the chemical and physical properties of DGEDDS/PDA and DGEDDS/MDA epoxy resins. *Journal of Materials and Environmental Science*, *1*(4), 277–288.

Reichmanis, E., Frank, C. W., O'Donnell, J. H., & Hill, D. J. T. (1993). *Radiation Effects on Polymeric Materials - A brief Overview*. 1–8. https://doi.org/10.1021/bk-1993-0527.ch001

Seifi, H., Gholami, T., Seifi, S., Ghoreishi, S. M., & Salavati-Niasari, M. (2020). A review on current trends in thermal analysis and hyphenated techniques in the investigation of physical, mechanical and chemical properties of nanomaterials. *Journal of Analytical and Applied Pyrolysis*, *149*(April), 14. https://doi.org/10.1016/j.jaap.2020.104840

Soares, J. M. A. A. (2021). *Effect of Gamma Irradiation on the Functional Properties of Epoxy Carbon-Fiber Reinforced Composite Material* (Issue May). Portuguese Air Force Academy.

Sun, Y., & Chmielewski, A. G. (2017). *Radiation processing of polymers in aqueous media. Applications of Ionizing Radiation in Materials Processing*. http://inis.iaea.org/search/search.aspx?orig_q=RN:46135064

Uthman, M., Shaibu, F., Bara'u Gafai, N., Labaran, I. F., Sadiq Umar, A., & Abdullahi, U. S. (2020). *5G Radiation and COVID-19: The Non-Existent Connection*. *8*, 34–38.

Wright, W. J., & Askeland, D. R. (2014). *The Science and Engineering of Materials 7th Edition*.

Yadav, V. S., Saxena, V., & Pandey, L. M. (2021). *Fiber Reinforced polymers : Processes and Applications* (C. I. P. S. Gürgen & E. Hoque (Eds.); Issue February). Nova Science Publishers.